ADVANCED MATERIALS
www.advmat.de

The Distance Between Phosphate-Based Polyanionic Compounds and Their Practical Application For Sodium-Ion Batteries

Zhiqiang Hao, Xiaoyan Shi, Zhuo Yang, Xunzhu Zhou, Lin Li, Chang-Qi Ma, and Shulei Chou**

Sodium-ion batteries (SIBs) are a viable alternative to meet the requirements of future large-scale energy storage systems due to the uniform distribution and abundant sodium resources. Among the various cathode materials for SIBs, phosphate-based polyanionic compounds exhibit excellent sodium-storage properties, such as high operation voltage, remarkable structural stability, and superior safety. However, their undesirable electronic conductivities and specific capacities limit their application in large-scale energy storage systems. Herein, the development history and recent progress of phosphate-based polyanionic cathodes are first overviewed. Subsequently, the effective modification strategies of phosphate-based polyanionic cathodes are summarized toward high-performance SIBs, including surface coating, morphological control, ion doping, and electrolyte optimization. Besides, the electrochemical performance, cost, and industrialization analysis of phosphate-based polyanionic cathodes for SIBs are discussed for accelerating commercialization development. Finally, the future directions of phosphate-based polyanionic cathodes are comprehensively concluded. It is believed that this review can provide instructive insight into developing practical phosphate-based polyanionic cathodes for SIBs.

1. Introduction

To achieve a green and sustainable society, the development of renewable energy sources (i.e., solar energy, tidal energy, and wind energy) is an inevitable trend. It is well known that the implementation of energy storage and conversion devices is a prerequisite for making the efficient utilization of renewable energy sources. In recent decades, lithium-ion batteries (LIBs) have dominated the battery market profiting from their relatively high energy density and long cycle life.[1] As the demand for energy storage systems in the energy market gradually tends to be on large-scale applications, the high cost and uneven geographical distribution of lithium resources result in LIBs no longer being ideally applicable to the needs of the future energy storage market.[2] Na^+ as the charge carrier for sodium-ion batteries (SIBs) exhibits significant economic advantages and promising physical properties compared to Li^+ (**Figure 1**a). In addition, SIBs show a similar working mechanism to LIBs (Figure 1b), and possess an abundance and uniform distribution of sodium resources. Therefore, SIBs with promising electrochemical performance gradually become a new favorite for large-scale energy storage in the battery market.

It is worth noting that SIBs are a beneficial complement, rather than replacement, to LIBs in the field of large-scale energy storage, so there is no fierce competitive relationship between the SIBs and LIBs. As shown in Figure 1c, the number of publications on SIBs increases yearly, suggesting SIBs as novel energy-storage devices have also caused extensive attention in academic circles. Nevertheless, the differences in charge carriers result in the electrode materials for SIBs not being able to completely replicate the successful electrode materials for LIBs. For instance, the commercial graphite anode for LIBs cannot be applied in SIBs, since the weak interaction between Na^+ and graphite layers makes it hard to form stable Na^+-graphite compounds.[3] Meanwhile, Na^+ is heavier and larger than Li^+, causing sluggish reaction kinetics and poor structural stability of SIBs during the charge/discharge process. Furthermore, the relatively high redox potential of Na^+/Na (−2.71 V vs −3.04 V for Li^+/Li, vs standard hydrogen electrode) means the lower energy density of SIBs than that of LIBs. Therefore, an essential need is to explore ideal electrode materials with a robust structure, fast electrochemical dynamics, and appropriate redox potential.

Z. Hao, X. Shi, Z. Yang, X. Zhou, L. Li, S. Chou
Institute for Carbon Neutralization
College of Chemistry and Materials Engineering
Wenzhou University
Wenzhou, Zhejiang 325035, China
E-mail: linli@wzu.edu.cn; chou@wzu.edu.cn
Z. Hao, X. Shi, Z. Yang, X. Zhou, L. Li, S. Chou
Wenzhou Key Laboratory of Sodium-Ion Batteries
Wenzhou University Technology Innovation Institute for Carbon Neutralization
Wenzhou, Zhejiang 325035, China
C.-Q. Ma
i-Lab & Printable Electronics Research Centre
Suzhou Institute of Nano-Tech and Nano-Bionics
Chinese Academy of Sciences (CAS)
Suzhou, Jiangsu 215123, China
The ORCID identification number(s) for the author(s) of this article can be found under https://doi.org/10.1002/adma.202305135

DOI: 10.1002/adma.202305135

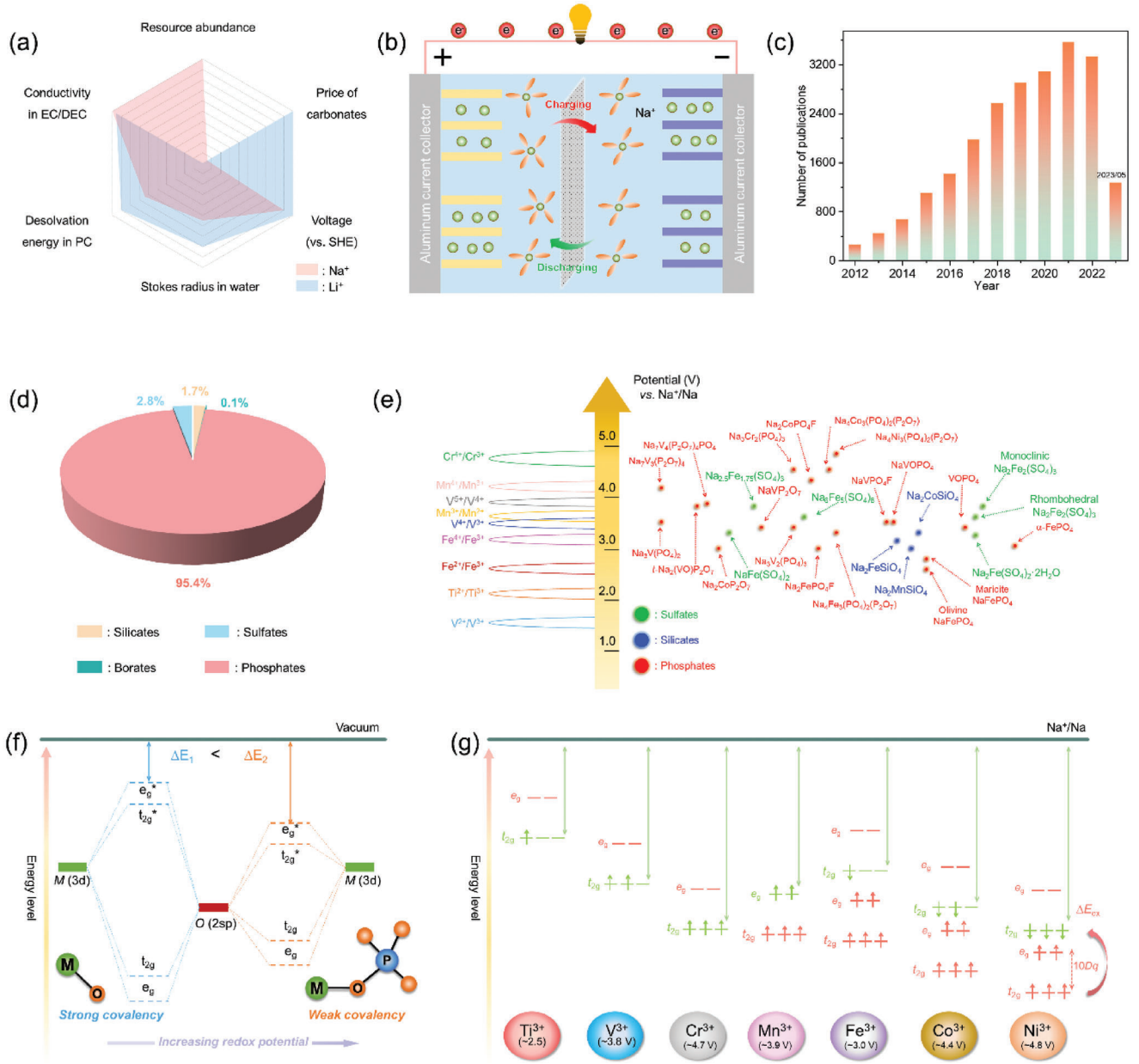

Figure 1. a) Properties of Li^+ and Na^+ as charge carriers for rocking-chair batteries and the price of the corresponding metals. b) Schematic illustration of SIBs' working mechanism. c) Publication numbers of SIBs collected from Web of Science in May 2023 (The keywords used for the search in the Web of Science were "Sodium-ion batteries," "Sodium metal battery," "Na-ion batteries," or "Sodium batteries"). d) The proportion of research on different types of polyanionic cathodes for SIBs was collected from the Web of Science in May 2023. e) Diagram of redox potentials of different transition metal species in $Na_xM_y(PO_4)_3$ system and the average voltages (vs Na^+/Na) of various polyanionic cathode materials. f) Schematic band structure for an oxide-based compound (left) and polyanionic compound (right) showing the influence of the polyanion on the ionicity of the M–O bond. g) Schematic comparison of operating voltages and *d*-electron configurations for phosphates with 3d transition metals. 10*Dq* and ΔE_{ex} indicate an octahedral crystal field splitting energy for 3d orbitals and exchange splitting energy, respectively.

From a commercial point of view, hard carbon (HC) anode for SIBs has exhibited excellent electrochemical performance and relatively low cost becoming the mainstream choice of anode for SIBs in start-up battery companies.[4–7] As for the cathode materials of SIBs, layered transition metal oxides, polyanionic compounds, and Prussian blue analogues (PBAs) are the mainstream for commercialization due to their superb sodium-storage performance.[8–11] In comparison with other cathode materials, polyanionic compounds possess relatively stable cycling performance, high working voltage, superior thermal stability, and remarkable safety.[12,13] Among the numerous polyanionic compounds (such as phosphates, sulfates, silicates, and borates), phosphate-based polyanionic compounds are the most widely studied polyanion framework of Na^+ (de)intercalation

due to their abundant species and variable average voltages (Figure 1d,e). The relevant chemical formula of phosphate-based polyanionic compounds can be summarized as $Na_xM_y(P_aO_b)_zY_w$ (M = V, Fe, Mn, Cr, Ti, Ni, etc.; Y = F, O, N, SO_4, CO_3, etc.), and the corresponding framework consists of $(P_aO_b)_z^{n-}$ polyhedral and MO_x polyhedral linked by strong covalent bonds, leading to remarkable stability.[14,15] Based on the molecular orbital principles, the covalent interaction between M and O leads to the split of molecular orbitals and the formation of bonding orbitals and antibonding orbitals. The splitting energy between antibonding and bonding orbitals can be high with the strong covalent properties of M–O, resulting in the decrease in energy difference between antibonding orbitals and vacuum (ΔE_1). Furthermore, the covalent properties of the M–O bond can be weakened by the introduction of atom P with strong electronegativity due to the generation of M–O–P, leading to the increase in energy difference between antibonding orbitals and vacuum (ΔE_2).[16] Therefore, phosphate-based polyanionic cathodes usually have a higher redox potential than layered transition metal oxides, as shown in Figure 1f. Meanwhile, the 3d transition metal ions (M^{n+}) with a larger effective nuclear charger with deeper valence levels tend to show higher $M^{(n+1)+}/M^{n+}$ redox potential, since the depth of the *3d* energy levels is up to the nuclear charge and valence number (Figure 1g). While the isolated electronic structure of transition metal ions in phosphate-based polyanionic compounds gives a high operating voltage, it can cause a low electric conductivity, further resulting in sluggish electrochemical kinetics.[17] Besides, the inactive polyanions in phosphate-based polyanionic compounds account for a significant proportion of the corresponding molecular weight, inevitably resulting in a relatively limited capacity. Many powerful modification strategies have been discovered to improve the electrochemical performance of phosphate-based polyanionic compounds, boosting their practical application potential.[18–22] Combining with suitable optimization methods, phosphate-based polyanionic compounds exhibit promising electrochemical performance, which has even begun to approach commercialization at the material level.

Herein, we aim to comprehensively review the development and the practical application potential of phosphate-based polyanionic compounds in the field of SIBs. First of all, the development history of high-performance phosphate-based polyanionic cathodes for SIBs is roughly summarized. Second, the crystalline structures and sodium-storage mechanisms of phosphate-based polyanionic compounds are discussed to provide an overall understanding. Subsequently, effective strategies are summarized to improve the performance of phosphate-based polyanionic compounds. Besides, we analyzed the practical application potential of phosphate-based polyanionic compounds for SIBs, based on the electrochemical performance and cost. Finally, the outlook and future perspectives of phosphate-based polyanionic cathodes are proposed. We believe that this review can provide constructive insights into the research and application of phosphate-based polyanionic cathodes for SIBs.

2. Development History of Phosphate-Based Polyanionic Cathode for SIBs

The types of phosphate-based polyanionic compounds generally include phosphates, pyrophosphates, and mixed phosphates. Among them, phosphates can be divided into Na superionic conductor (NASICON)-type phosphates and $NaMPO_4$. In general, the $(P_aO_b)_z^{n-}$ polyhedral in phosphate-based polyanionic compounds acts as a 3D skeleton to stabilize the crystalline structure of phosphate-based polyanionic compounds, and these oxygen atoms are also bound by strong covalent bonds in $(P_aO_b)_z^{n-}$ polyhedral, revealing the potential of good cycling/rate performance. The general development history of phosphate-based polyanionic compounds for SIBs is shown in **Figure 2**a. As early as 1992, Gopalakrishnan et al. proved the reversible Na^+-(de)insertion of $V_2(PO_4)_3$, suggesting the potential of phosphates for sodium storage.[23] However, until 2002, phosphate-based polyanionic compound ($NaVPO_4F$) was first used for SIBs and showed good sodium-storage performance.[24] Subsequently, $Na_3(VO_{1-x}PO_4)_2F_{1+2x}$-type cathodes were also reported, which possess high average voltages, large specific capacities, and superior cycle life.[25,26] To further highlight the low-cost advantages of SIBs, drawing on the experience of LIBs, some Fe-based phosphates (i.e., Na_2FePO_4F and olivine $NaFePO_4$) were also applied to SIBs, and have large specific capacities and stable charge/discharge plateaus.[27–29] In addition, some pyrophosphates and pyrophosphate-phosphate mixed polyanionic compounds were also reported continuously, including $Na_2FeP_2O_7$, $Na_4Fe_3(PO_4)_2P_2O_7$, $Na_2MnP_2O_7$, $Na_4Co_3(PO_4)_2P_2O_7$, $Na_7V_4(P_2O_7)_4PO_4$, etc.[30–35] Considering the undesirable capacities of phosphate-based polyanionic compounds, NASICON-type phosphates with binary transition metal (i.e., $Na_3MnTi(PO_4)_3$, $Na_4MnV(PO_4)_3$, and $Na_2TiV(PO_4)_3$) have been developed to achieve large specific capacity by adjusting the potential window, but this may result in poor cycling stability.[36–38] Recently, the high-entropy phosphate of $Na_{3.4}Fe_{0.4}Mn_{0.4}V_{0.4}Cr_{0.4}Ti_{0.4}(PO_4)_3$ has been reported for SIBs, which shows better electrochemical performance than the monometallic phosphates, mainly due to the more stable crystal structure and better electrochemical activity.[3] The proportion of various phosphate-based polyanionic cathodes for SIBs is illustrated in Figure 2b, and the research on NASICON-type phosphates is dominant benefiting from their excellent sodium-storage performance. Especially, NASICON-type phosphates (i.e., $Na_3V_2(PO_4)_3$ and $Na_3(VO_{1-x}PO_4)_2F_{1+2x}$) have been popular since their initial use as the cathode for SIBs owing to their excellent ionic conductivity, stable structure, and high operation voltage. Meanwhile, more Fe-based phosphates with low cost are reported and show remarkable electrochemical performance, including $Na_4Fe_3(PO_4)_2P_2O_7$, nanosized maricite $NaFePO_4$, and Na_2FePO_4F.[20] Nevertheless, Mn-based phosphate as another low-cost cathode for SIBs suffers from the Jahn-Teller effect of Mn^{3+} under high potential, limiting their advantages of high energy density. Noticeably, to demonstrate the commercial potential of such cathode materials for SIBs, some phosphate-based polyanionic compounds have achieved mass synthesis on the laboratory scale (Figure 2c).[39–41]

As known, energy density is the primary challenge to be solved for enhancing the practicality of phosphate-based polyanionic cathodes. Figure 2d illustrates that the theoretical energy density depends on the number of transition electrons, discharge voltage, and the molecular weight of the electrode material. Although phosphate-based polyanionic cathodes possess relatively large molecular weights, their higher operation voltages can

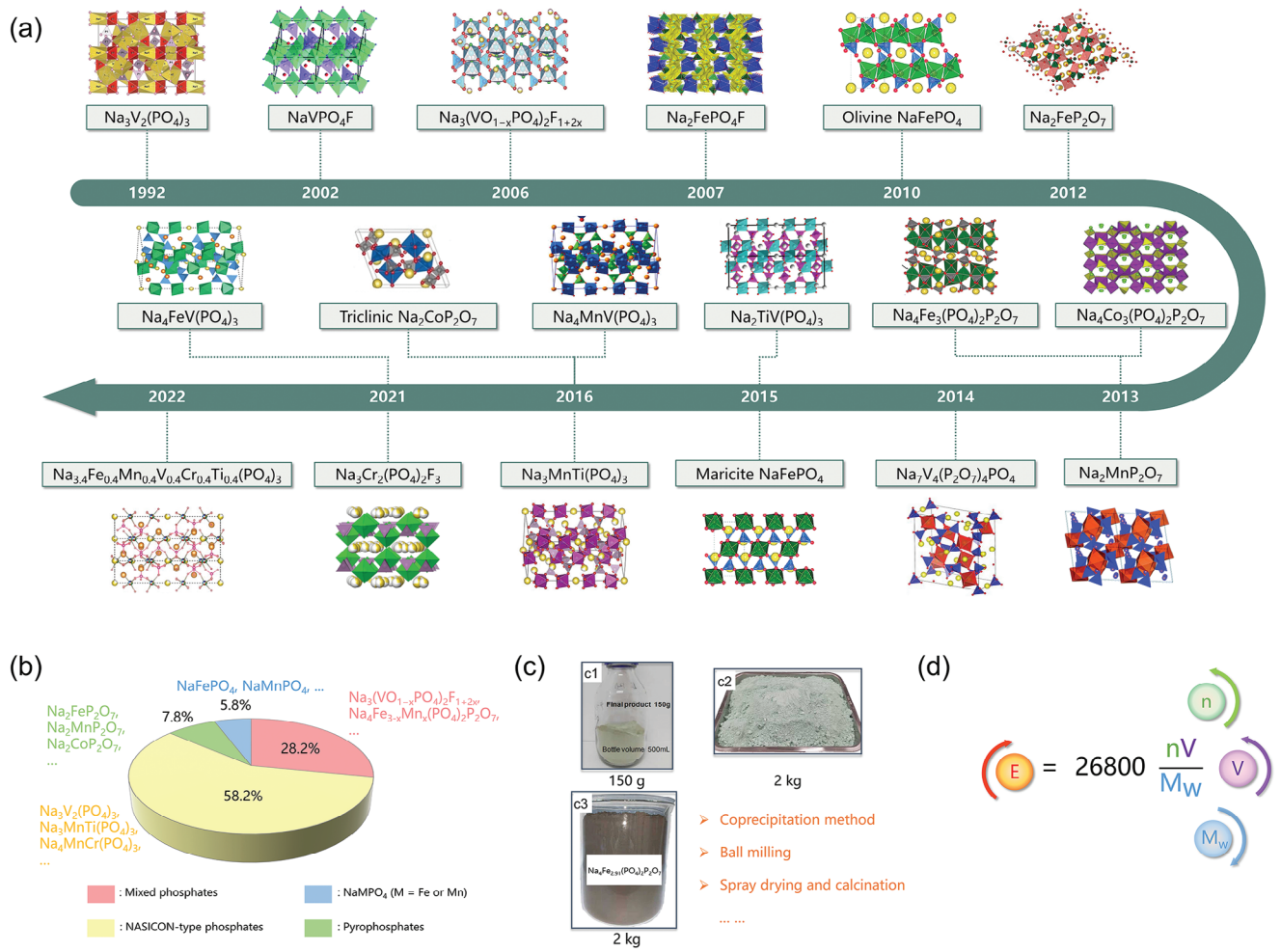

Figure 2. a) The development process of phosphate-based polyanionic cathodes for SIBs. b) The proportion of research on different phosphate-based polyanionic cathode materials for SIBs was collected from the Web of Science in April 2023. c) Reported large quantities of phosphate cathodes and potential synthesis methods for commercialization. Reproduced with permission.[39–41] c1) Reproduced with permission.[39] Copyright 2018, Elsevier. c2) Reproduced with permission.[40] Copyright 2022, American Association for the Advancement of Science. c3) Reproduced with permission.[41] Copyright 2021, Elsevier. d) The formula to calculate the energy density of different electrode materials, *E*: energy density (Wh kg^{-1}), *n*: the number of transferred electrons from one molecule, *V*: operation voltage (V), and M_w: molecular weight (g mol^{-1}).

offset the shortage to a large degree, obtaining a pretty good energy density. In general, the operation voltages of phosphate-based polyanionic compounds are up to the types of both anions and transition metal ions. For instance, the discharge plateau of olivine $NaFePO_4$ is ≈2.75 V, whereas both the discharge plateaus of Na_2FePO_4F and $Na_2FeP_2O_7$ are as high as ≈3.0 V.[42–44] The average voltage of $NaFe_2PO_4(SO_4)_2$ can also reach 3.4 V, which further suggests the importance of anions for operation voltages.[45] This phenomenon can be attributed to the variety of electrochemical negativity of different anions. Besides, for different transition metal species in phosphates, the operation voltage of $Na_3V_2(PO_4)_3$ is much higher than that of $Na_3Fe_2(PO_4)_3$ (3.4 V vs 2.6 V), since V^{3+} has a larger effective nuclear charge with deeper valence levels tend than that of Fe^{2+} (Figure 1g).[46,47] Considering the respective superiorities of metal species and anions, Yamada's group synthesized the cathodes of $Na_3Cr_2(PO_4)_3$ and $Na_3Cr_2(PO_4)_2F_3$, which possess ultrahigh and stable operation voltages of 4.5 and 4.7 V, respectively, based on the redox couple of Cr^{4+}/Cr^{3+}.[48,49] However, their practical capacities and cycling properties are not good enough probably due to poor electrochemical activity and the decomposition of electrolytes at high voltage.

3. Recent Progress of Phosphate-Based Polyanionic Cathodes for SIBs

3.1. Phosphates

3.1.1. NASICON-Type Phosphates

NASICON-type phosphates as the typical cathode for SIBs can be defined as $Na_xM(PO_4)_3$ ($1 \leq x \leq 4$; M = V, Ti, Cr, Fe, Ni, Co, etc.), and the corresponding crystal framework generally consists of two MO_6 octahedron units sharing the corners with three PO_4 tetrahedral units. This open crystalline structure offers easily accessible Na^+ transport channels,

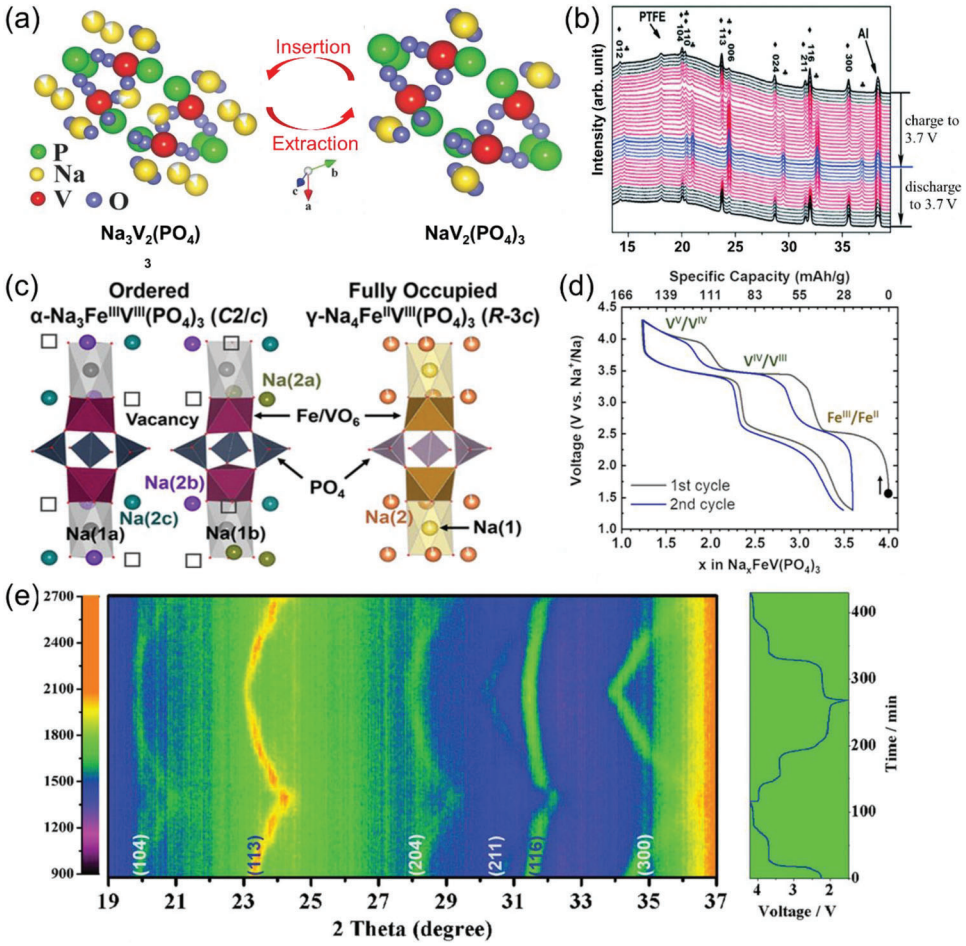

Figure 3. a) Schematic diagram of crystalline structural phase transition of $Na_3V_2(PO_4)_3$ with the Na^+ extraction/insertion. Reproduced with permission.[51] Copyright 2014, Wiley-VCH. b) In situ XRD patterns of the $Na_3V_2(PO_4)_3$ cycled in the range of 2.7–3.7 V (vs Na^+/Na) at 0.1 C (◆: $Na_3V_2(PO_4)_3$, ♣: $NaV_2(PO_4)_3$). Reproduced with permission.[52] Copyright 2013, Wiley-VCH. c) Schematic representations of Na^+ distributions in $Na_3FeV(PO_4)_3$ and $Na_4FeV(PO_4)_3$. d) Voltage-composition electrochemical curves of the $Na_4FeV(PO_4)_3$ during the first two cycles with a voltage window of 1.3–4.3 V (vs Na^+/Na) at 0.05 C. Reproduced with permission.[56] Copyright 2021 American Chemical Society. e) In situ XRD patterns of the $Na_3MnTi(PO_4)_3$ in the potential window of 1.5–4.2 V (vs Na^+/Na) at 50 mA g^{-1}. Reproduced with permission.[58] Copyright 2019, Wiley-VCH.

suggesting the potential for outstanding electrochemical kinetics. Meanwhile, NASICON-type phosphates also exhibit excellent material diversity owing to the substitutability of transition metal ions with different valence states.[50] Among various NASICON-type phosphates, $Na_3V_2(PO_4)_3$ stands out due to its relatively high redox potential, large theoretical capacity, and ultra-stable crystalline structure. Its crystalline structure belongs to rhombohedral (space group: *R*-3*c*), and Na^+ has two positions of Na1 site with a six-fold coordination and Na2 site with an eight-fold coordination in $Na_3V_2(PO_4)_3$, respectively. In 2014, Jian et al. calculated the occupancy rates of Na1 (0.8430) and Na2 (0.7190) in $Na_3V_2(PO_4)_3$ according to the Rietveld-refined X-rays diffraction (XRD) patterns of $Na_3V_2(PO_4)_3$.[51] As shown in **Figure 3**a, no Na single can be checked in Na2 site due to the completely out of its Na^+ after two Na^+ extraction from $Na_3V_2(PO_4)_3$, but the occupancy rate of the Na1 site remains unchanged compared with the initial state of $Na_3V_2(PO_4)_3$. These results indicate the capacity of $Na_3V_2(PO_4)_3$ is mainly contributed by the extraction/intercalation of Na^+ located in Na2 site corresponding to V^{4+}/V^{3+} redox couple with a theoretical capacity of 117 mAh g^{-1}. The related volume change from $Na_3V_2(PO_4)_3$ to $NaV_2(PO_4)_3$ is only 8.26%, and the related sodium-storage process is a typical two-phase reaction, as shown in Figure 3b.[52] Besides, Dominko et al. observed the V valence state and local symmetry during 2.0–4.0 V through in situ K-edge X-ray absorption near edge structure (XANES), and there is only a small change in the average bond length between V and O atoms in the first coordination.[53] The phenomena suggest that $Na_3V_2(PO_4)_3$ crystal structure is stable and reversible with the (de)intercalation of Na^+. Since the average voltage is essential for the energy density of SIBs, the NASICON-type $Na_3Cr_2(PO_4)_3$ (Rhombohedral, space group: *R*-3*c*) with a high and stable operation voltage of 4.5 V (Cr^{4+}/Cr^{3+}) was synthesized by Yamada's group.[49]

Considering the toxicity and high cost of V and Cr, some non-toxic and resources-rich metal elements (i.e., Fe, Ti, and Mn) are used to substitute partially/all V in $Na_3V_2(PO_4)_3$, including $Na_2TiV(PO_4)_3$, $Na_4MnV(PO_4)_3$, $Na_3FeV(PO_4)_3$, $Na_4FeV(PO_4)_3$,

$Na_3MnTi(PO_4)_3$, $Na_4MnCr(PO_4)_3$, etc.[38,54–57] These NASICON-type cathode materials with binary transition metals almost exhibit promising sodium-storage properties, such as large reversible capacities and high operation voltages.[58–60] In 2015, Mason et al. first reported the binary transition metal type NASICON material of $Na_2TiV(PO_4)_3$.[37] Then, Du et al. found that $Na_2TiV(PO_4)_3$ (*R*-3*c*) can deliver a large reversible capacity of 147 mA h g^{-1} at 0.1 C during 1.5–4.5 V through the redox couples of V^{4+}/V^{3+}, Ti^{4+}/Ti^{3+}, and V^{3+}/V^{2+}.[61] Furthermore, the sodium-storage process of $Na_2TiV(PO_4)_3$ was revealed by in situ synchrotron XRD, which includes stepped solid-solution and two two-phase reactions. Similarly, Goodenough's group first investigated the crystalline structure and properties of $Na_4MnV(PO_4)_3$ and $Na_3FeV(PO_4)_3$.[36] The $Na_4MnV(PO_4)_3$ with a space group of *R*-3*c* has two types of independent Na^+ with different oxygen environments, locating in the interstitial space of the framework, one for 6-fold coordination (Na1), and the other one three for 10-fold coordination (Na2) per formula unit. However, the crystalline structure of $Na_3FeV(PO_4)_3$ shows a little difference from $Na_4MnV(PO_4)_3$ due to the cooperative distortion of the FeO_6 octahedron, distorting the crystal structure to monoclinic in a space group of *C*/2*c*. Both $Na_4MnV(PO_4)_3$ and $Na_3FeV(PO_4)_3$ exhibit two distinctive plateaus, centering at 3.2–3.4 V (V^{4+}/V^{3+}), 3.5–3.6 V (Mn^{3+}/Mn^{2+}), or 2.4–2.7 V (Fe^{3+}/Fe^{2+}).

Subsequently, Masquelier et al. further explored the crystal chemistry of NASICON-type $Na_4FeV(PO_4)_3$ (Rhombohedral, space group: *R*-3*c*) and $Na_3FeV(PO_4)_3$ (Monoclinic, Space group: *C*/2*c*), as shown in Figure 3c.[56] The unit cell volume of $Na_4FeV(PO_4)_3$ is 3.4% larger than that of $Na_3FeV(PO_4)_3$ because of one additional Na^+ insertion. Within the potential window of 1.3-4.3 V (vs Na^+/Na), $Na_4FeV(PO_4)_3$ allows the electrochemical extraction of 2.76 Na^+ (156 mAh g^{-1}) due to the activation of the redox couples of Fe^{3+}/Fe^{2+}, V^{4+}/V^{3+}, and V^{5+}/V^{4+} (Figure 3d). Similarly, the V^{5+}/V^{4+} redox couple can also be activated by the Mn-substituted $Na_3V_2(PO_4)_3$ ($Na_4MnV(PO_4)_3$), obtaining a large specific capacity and high energy density.[22] Besides, $Na_3MnTi(PO_4)_3$ as the isostructure of $Na_3V_2(PO_4)_3$ is a typical rhombohedral lattice in the space group *R*-3*c*, and has a framework formed by corner-sharing MnO_6 or TiO_6 octahedral and PO_4 tetrahedral units with large open channels. Generally, the Mn-based polyanionic cathode compounds suffer from serious structure distortion due to the Jahn-Teller effect of Mn^{3+} within the (de)sodiation process, whereas the 50% of Ti^{4+} can stabilize the crystalline structure of $Na_3MnTi(PO_4)_3$, leading to a stable framework. The sodium-storage mechanism of $Na_3MnTi(PO_4)_3$ was investigated by Zhou et al., and they found the specific capacity is mainly contributed by the redox couples of Mn^{3+}/Mn^{2+} and Mn^{4+}/Mn^{3+} during the voltage range of 2.5–4.2 V.[58] According to the in situ XRD result, the (de)sodiation process of $Na_3MnTi(PO_4)_3$ exhibits excellent reversibility and consists of solid-solution and two-phase reaction (Figure 3e). Due to the electrochemical activity of Ti at ≈2.0 V (vs Na^+/Na), it is possible for the three-electron reactions via expanding the voltage range, such as 1.3–4.3 V. Currently, many works have demonstrated the feasibility of $Na_3MnTi(PO_4)_3$ as the cathode with high specific capacity.[62,63]

The low-cost NASICON-type $Na_3Fe_2(PO_4)_3$ (Monoclinic, space group: *C*2/*c*) was first reported by Dou's group, and shows a high capacity retention of >96% after 200 cycles.[64] Subsequently, Xia et al. designed a flake porous $Na_3Fe_2(PO_4)_3$ cathode material with a large reversible capacity of 100.8 mAh g^{-1} at 0.1 C.[65] Although $Na_3Fe_2(PO_4)_3$ has a relatively large specific capacity, its low average voltage (<3.0 V) makes it limited in development. Briefly, $Na_3V_2(PO_4)_3$ is a promising cathode active material for SIBs, whereas the high cost and toxicity of V resources limit its commercial development. Fortunately, more and more works have found that the NASICON-type materials with superior electrochemical performance can also be obtained by using low-cost, green, and environmentally friendly metal elements to completely/partially replace V, which provides more choices for the cathode of SIBs in the future.[12]

3.1.2. $NaMPO_4$

Inspired by olivine $LiFePO_4$ in the system of LIBs, the sodium-storage performance of $NaFePO_4$ is also investigated in the system of SIBs.[66] Differing from $LiFePO_4$, the crystalline structures of $NaFePO_4$ include olivine phase and maricite phase (**Figure 4**a).[27] However, the maricite $NaFePO_4$ is the thermally stable phase under high temperatures (> 480 °C). The olivine $NaFePO_4$ has an orthorhombic lattice with a space group of *Pmmb*, and its framework consists of slightly distorted FeO_6 octahedra and PO_4 tetrahedra. Namely, corner-shared FeO_6 octahedra in the *bc* plane and edge-shared NaO_6 octahedra in a direction along the *b*-axis are linked by edge/corner-shared PO_4 tetrahedra, creating a stable 1D channel for Na^+ migration. Hence, olivine $NaFePO_4$ is electrochemically active for sodium storage with a large theoretical capacity of 154 mAh g^{-1}. The sodium-storage mechanism of olivine $NaFePO_4$ was revealed by Boucher's group.[27,67] They found the olivine $NaFePO_4$ possesses two significant plateaus during the desodiation process, but only shows one plateau with the insertion of Na^+, as shown in Figure 4b. This can be attributed to the existence of ordered $Na_{2/3}FePO_4$ intermediate, so the desodiation process of olivine $NaFePO_4$ is not a single two-phase reaction. The solid-solution reaction occurs during the (dis)charging process due to the large solid solubility of Na^+/vacancy of Na_xFePO_4 ($2/3 < x < 1$), and the (de)sodiation process in $0 < x < 2/3$ corresponds to the two-phase reaction between $Na_{2/3}FePO_4$ and $FePO_4$. Meanwhile, the full Na in olivine $NaFePO_4$ can be reversibly inserted and extracted with a volume change of 17.58%.[68] Noticeably, Loh and co-workers demonstrated that olivine $NaFePO_4$ obtained by aqueous ion exchange shows more remarkable electrochemical properties (142 mA h g^{-1} at 0.1 C and 92% capacity retention after 200 cycles) than that prepared by organic ion exchange.[69] Furthermore, they also explained the reason why only one plateau during the discharge process in detail through in situ synchrotron Fe K-edge XANES (Figure 4c–f). This can be assigned to the overlap of the discharge plateau from $FePO_4$ to $Na_{2/3}FePO_4$ (sluggish reaction kinetics) and the discharge plateau from $Na_{2/3}FePO_4$ to $NaFePO_4$ (fast reaction kinetics). Nevertheless, all reported synthesis methods of olivine $NaFePO_4$ are still relatively complex and specifically, including the electrochemical delithiation of $LiFePO_4$ to obtain $FePO_4$ and the electrochemical sodiation of $FePO_4$ to obtain $NaFePO_4$.[66] Hence, it is critical to achieving the mass production of olivine $NaFePO_4$ via a facile method.

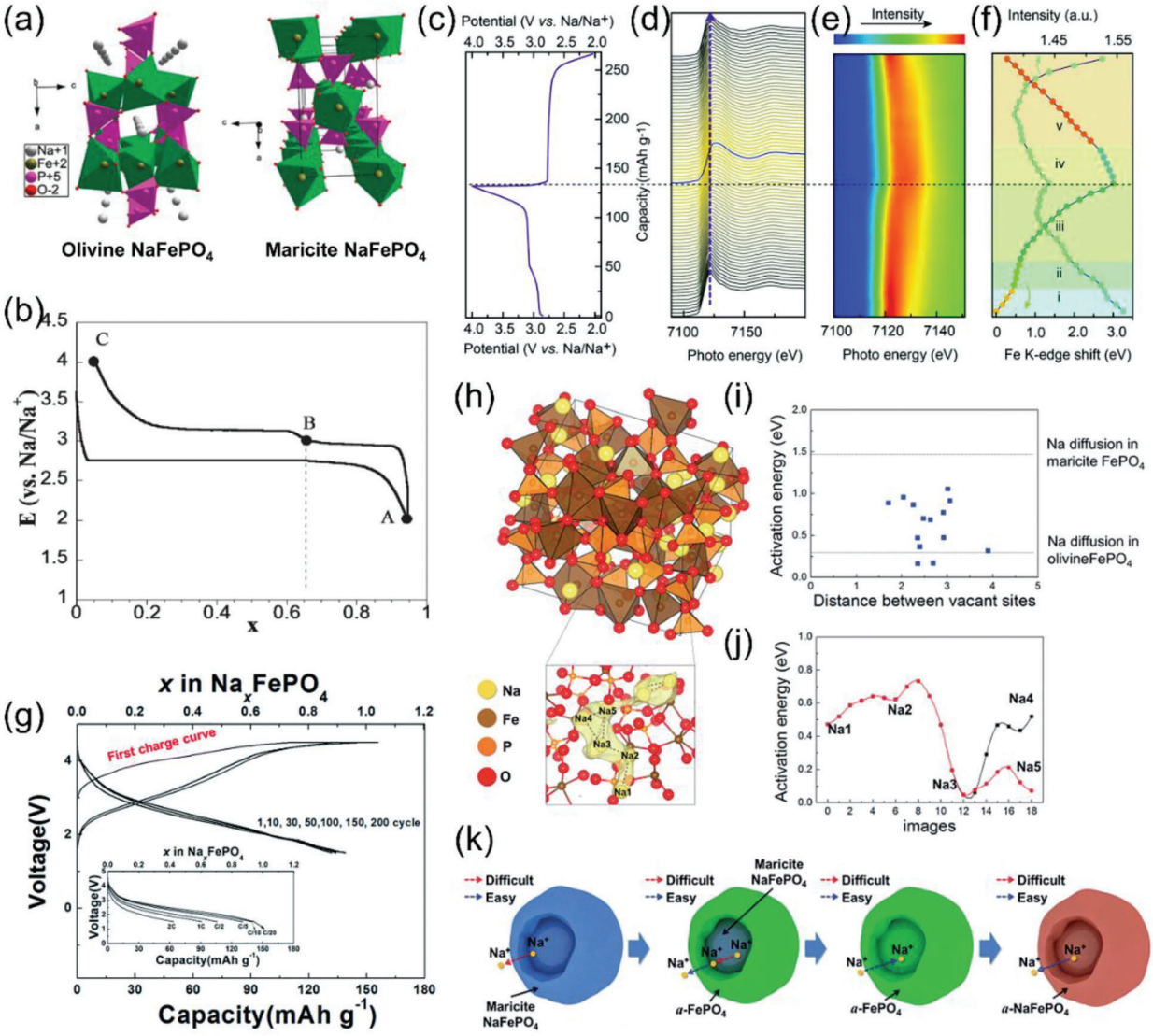

Figure 4. a) Structures of maricite $NaFePO_4$ and olivine $NaFePO_4$. b) The typical electrochemical curve for the synthesis of $NaFePO_4$ and $Na_{0.7}FePO_4$ in PITT mode. Reproduced with permission.[27] Copyright 2010, American Chemical Society. c) Voltage profile of the $NaFePO_4$ at the first cycle, d) stacking plots, e) 2D contour plots, and f) the evolution of the Fe-edge energy (half weight) of operando XANES spectra of the $NaFePO_4$ at the first cycle. Reproduced with permission.[69] Copyright 2016, The Royal Society of Chemistry. g) Galvanostatic curves of maricite $NaFePO_4$ at 0.05 C (inset is the discharge curves of maricite $NaFePO_4$ at different C-rates). h) Plausible Na sites and diffusion pathways of a-$FePO_4$, i) activation energies of Na hopping between Na sites as a function of distance between Na sites, and j) the activation energies for Na diffusion along Na1–Na2–Na3–Na4/Na5 diffusion pathways (over 10 Å) in a-$FePO_4$. k) Schematic representation of the electrochemical mechanism during charge/discharge cycling in maricite $NaFePO_4$. Reproduced with permission.[29] Copyright 2015, The Royal Society of Chemistry.

For maricite $NaFePO_4$, the sites of Na^+ and Fe^{2+} are the opposite of those in olivine $NaFePO_4$, with the PO_4 site remaining unchanged. This change leaves the structure devoid of migration tunnels for Na^+, resulting in the theoretically electrochemical inactivity of maricite $NaFePO_4$. However, Kang et al. demonstrated that the nanosized maricite $NaFePO_4$ can also achieve the reversible insertion/extraction of Na^+ (142 mAh g^{-1} at 0.05 C; capacity retention of 95% after 200 cycles), as shown in Figure 4g.[29] This unexpected result is contributed by the Na^+ extraction from nanosized maricite $NaFePO_4$ is accompanied by the transformation into amorphous $FePO_4$ (a-$FePO_4$). Meanwhile, Figure 4h–j illustrate that the activation energies for Na hopping in a-$FePO_4$ is ≈0.73 eV along the pathways of Na1–Na2–Na3–Na4/Na5 (≈1 nm), much less than that in the maricite phase (≈2.68 eV) based on the Quantum mechanics calculations, leading to the increase in the Na diffusion under normal battery operation conditions. Figure 4k vividly displays the sodium-storage process of maricite $NaFePO_4$ with the (de)intercalation of Na^+. Recently, Vlad et al. also investigated the off-stoichiometric iron-rich $Na_{0.6}Fe_{1.2}PO_4$ (0.4 Na^+ being replaced by 0.2 Fe^{2+}) as the cathode for SIBs, which show superb sodium-storage properties (350 Wh kg^{-1}, 97.3 mAh g^{-1} at 2 C after 2000 cycles).[70] These authors found an interesting

phenomenon that a reversible plateau occurs after 1000 cycles, enhancing the energy and power densities, whereas no reaction mechanism was proposed.

Similar to $NaFePO_4$, the phases of $NaMnPO_4$ also include olivine structure and maricite structure, but the sodium-storage properties of either the maricite phase or olivine phase are relatively poor.[71] According to the relevant density functional theory (DFT) calculation, the theoretical operating voltage of $NaMnPO_4$ is higher than the oxidation decomposition potential of common electrolytes, so $NaMnPO_4$ generally shows weak sodium-storage capability.[72] As far as the current research is concerned, $NaMnPO_4$ as a cathode is unsuitable for SIBs because of the undesirable sodium-storage performance. Besides, Ceder et al. calculated the theoretical output voltages of olivine/maricite NaNiPO4 (4.58 and 4.94 V) and olivine/maricite NaCoPO4 (4.19 and 4.09 V), but their electrochemical activities have never been verified experimentally.[73]

3.2. Pyrophosphates

Pyrophosphates as the analogue of phosphates show better thermal stability and crystallinity than phosphates because $P_2O_7^{4-}$ is generally derived from the decomposition and deoxidation of PO_4^{3-} under high temperatures (500–550 °C).[74] Meanwhile, the framework of pyrophosphate is comprised of transition metal octahedral MO_6 and P_2O_7 units, forming interconnected channels for Na^+ migration. In the pyrophosphate-based cathode for SIBs, two-sodium metal pyrophosphates ($Na_2MP_2O_7$, M = Fe, Mn, V, Co, etc.) are the principal research object, and the corresponding crystalline structures include triclinic, tetragonal, orthorhombic, and monoclinic phases.[75] Among them, triclinic $Na_2FeP_2O_7$ (Space group: *P*-1) has the specific lattice parameters of a = 6.434 Å, b = 9.416 Å, c = 11.018 Å, α = 64.409°, β = 85.479°, γ = 72.807°.[44] The crystal structure of $Na_2FeP_2O_7$ contains corner-sharing Fe_2O_{11} dimers and P_2O_7 units, linked by corner-sharing and edge-sharing fashion. In 2012, Barpanda et al. first reported $Na_2FeP_2O_7$ cathode for SIBs with a high operation voltage of 3.0 V (vs Na^+/Na) and a large theoretical capacity of 100 mAh g^{-1}, based on the Fe^{3+}/Fe^{2+} redox couple.[76] Subsequently, they found the desodiated $NaFeP_2O_7$ just show irreversible phase transition (*P*-1 → $P2_1/c$) without thermal decomposition and/or oxygen evolution below 600 °C, suggesting the outstanding thermal stability and high safety of $Na_2FeP_2O_7$.[44] To investigate the sodium-storage process of $Na_2FeP_2O_7$, Kim et al. combined experimental and theoretical study, including ex situ XRD and DFT calculations.[77] In the initial charge/discharge stages, the sodium-storage reactions can be divided into solid-solution reaction (≈2.5 V) and two-phase reaction (3.0–3.25 V), involving various intermediate phases from 2.0 to 4.5 V (**Figure 5**a). Meanwhile, according to the DFT calculation, the 2.5 V plateau can be attributed to the Na extraction at the Na1 site due to its higher energy and lower migration energy barriers than Na2–Na8 sites, and the plateaus around 3.0 V are assigned to the extraction of Na in Na3–Na8 sites by 1D or/and 2D paths (red line), as shown in Figure 5b. As known, only the Fe^{3+}/Fe^{2+} couple participates in the redox reaction, resulting in the gain/loss of one electron, while both Na^+ in $Na_2FeP_2O_7$ can be reversibly inserted/extracted. Therefore, to achieve the reversible insertion/extraction of more Na^+, a series of nonstoichiometric $Na_{4-2x}Fe_{2+x}(P_2O_7)_2$ ($0 < x < 1$) compounds were also developed by coordinating the balance between Fe^{2+} and Na^+, such as $Na_{3.32}Fe_{2.34}(P_2O_7)_2$, $Na_{3.12}Fe_{2.44}(P_2O_7)_2$, and $Na_7Fe_{4.5}(P_2O_7)_4$.[9,78–80] These nonstoichiometric Fe-based pyrophosphates display relatively large specific capacity and stable cycling performance, suggesting the positive effect of adjusting Fe content on the sodium-storage performance.

Figure 5c illustrates that the triclinic phase of $Na_2MnP_2O_7$ with a space group of *P*-1 has larger lattice parameters than those of $Na_2FeP_2O_7$ due to the larger Mn^{2+} (0.83 Å vs 0.78 Å of Fe^{2+}).[81] For the first time, Choi et al. reported the specific capacity of $Na_2MnP_2O_7$ can reach 90 mAh g^{-1} with a high redox activity center at 3.8 V (Mn^{3+}/Mn^{2+}), and its capacity retention is 70% with an increase in current density from 0.05 to 1 C at room temperature.[82] The excellent rate performance of $Na_2MnP_2O_7$ is beneficial from the locally flexible accommodation of Jahn–Teller distortions drawing support from the corner-sharing crystalline structure in the triclinic phase, according to DFT calculations. Almost simultaneously, Yamada's group unveiled β-$Na_2MnP_2O_7$ (space group: *P*1), which has a high redox potential of 3.6 V according with DFT calculations, as shown in Figure 5d.[32] At a rate of 0.05 C, the reversible capacity of β-$Na_2MnP_2O_7$ is also up to 80 mAh g^{-1}. In addition, Jiao et al. modified the sodium-storage performance of $Na_2MnP_2O_7$ using graphene layers as the carbon matrix, and its capacity retention can reach 83% at 2 C over 600 cycles.[81]

Differing from $Na_2FeP_2O_7$ and $Na_2MnP_2O_7$, the crystalline phases of $Na_2CoP_2O_7$ include orthorhombic (Space group: *Pna*2), tetragonal (space group: $P42/mnm$), and triclinic (space group: *P*-1) since Co can be either tetrahedrally coordinated or octahedrally coordinated. The crystalline structure of orthorhombic $Na_2CoP_2O_7$ consists of parallel slabs of mixed CoO_4 and PO_4 to assemble $[Co(P_2O_7)]^{-2}$ layers in parallel with (001). Meanwhile, $[Co(P_2O_7)]^{-2}$ layer and Na layer are alternately stacked to form a contract structure. The electrochemical performance of orthorhombic $Na_2CoP_2O_7$ cathode with a layered structure was systematically investigated by Yamada's group.[83] The specific capacity of $Na_2CoP_2O_7$ is only 80 mAh g^{-1} with a low average voltage of 3.0 V, corresponding to the Co^{3+}/Co^{2+} redox couple. Nevertheless, Jung and co-workers achieved the defect-controlled formation of triclinic $Na_2CoP_2O_7$ (Space group: *P*-1) with a stable rose phase (Figure 5e), which possesses a relatively high discharge voltage of 4.3 V (Figure 5f).[35] Its energy density is as high as 344 Wh kg^{-1}, much better than layered $Na_2CoP_2O_7$, revealing the selection of crystalline structure significantly affects the electrochemical behavior of $Na_2CoP_2O_7$. Taking into consideration of cost and electrochemical performance, $Na_2CoP_2O_7$ is not an ideal cathode for SIBs. Besides, some novel pyrophosphates were also reported and have a relatively high average voltage, such as $Na_7V_3(P_2O_7)_4$, $Na_{3.12}Fe_{2.44}(P_2O_7)_2$, and $Na_7Fe_{4.5}(P_2O_7)_4$ etc.[79,84–86]

3.3. Mixed Phosphates

In general, the electronegativity of anions in polyanionic compounds is closely related to the covalent property of M–O, further affecting the operation voltage of polyanionic cathodes.

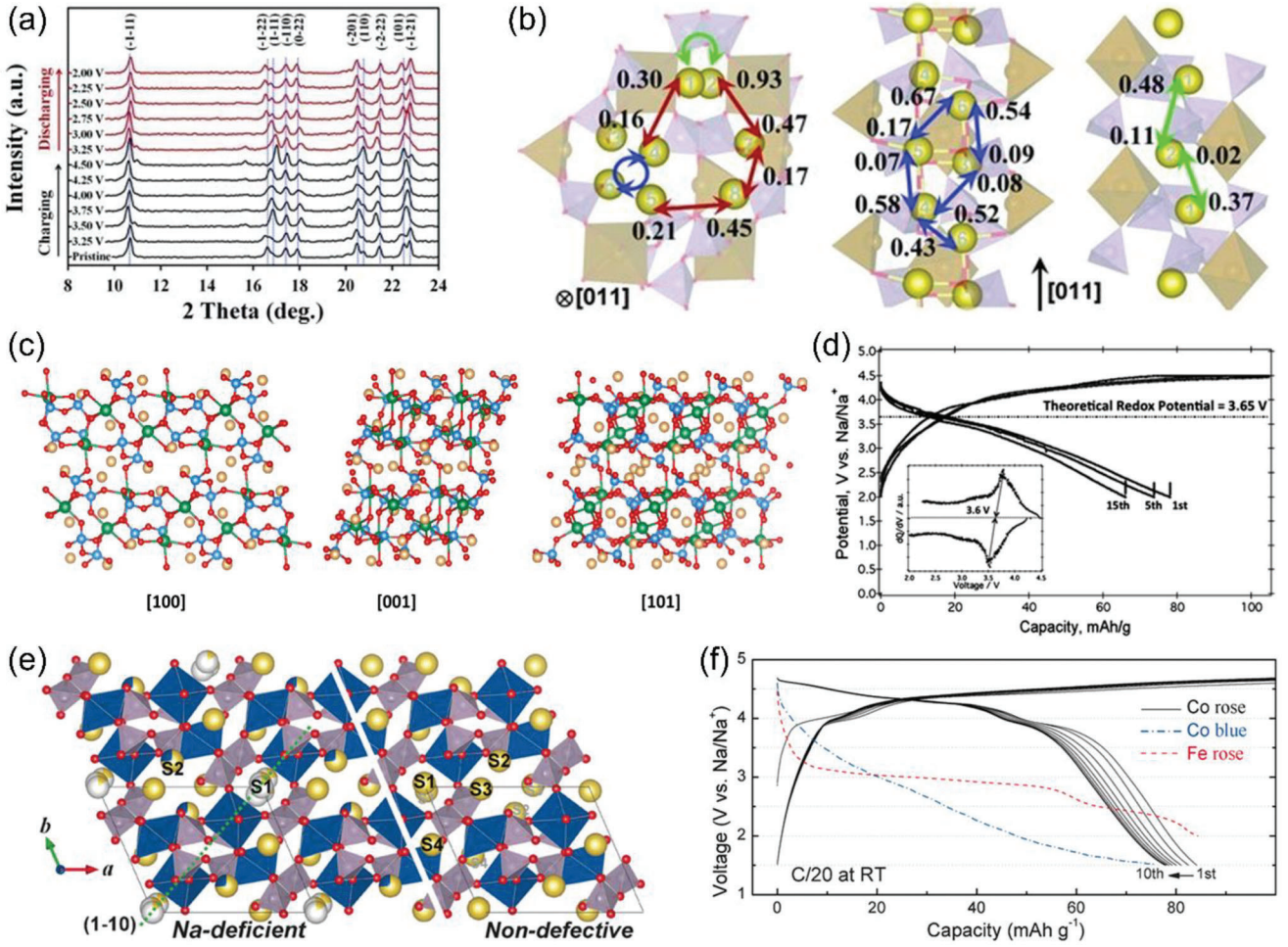

Figure 5. a) Electrochemical ex situ XRD analyses data of $Na_2FeP_2O_7$ in the first charging and discharging processes. b) The calculated Na ion migration barriers (in eV) for the $Na_2FeP_2O_7$. The arrowhead and the number next to it indicate the direction of Na-migration and the corresponding migration barrier (either forward or backward). Reproduced with permission.[77] Copyright 2013, Wiley-VCH. c) Schematic illustrations of the $Na_2MnP_2O_7$ crystal framework with spacious ion diffusion channels along the [100, 001] and [101] directions. The atoms of Na (yellow), P (blue), Mn/V (green), and O (red) are shown.[81] Copyright 2013, The Royal Society of Chemistry. d) Galvanostatic voltage–capacity profiles of the β-$Na_2MnP_2O_7$ cathode at 0.05 C, and the inset image shows the differential capacity (dQ/dV) plot. Reproduced with permission.[32] Copyright 2013, The Royal Society of Chemistry. e) Refined Na-deficient crystal structure of the synthesized Co rose phase (left) and a hypothetical Co rose phase without defects (right). Co blue, Na yellow, O red, P gray, vacancies white. f) Galvanostatic cycles of the Co rose, Fe rose, and Co blue polymorphs. Reproduced with permission.[35] Copyright 2016, Wiley-VCH.

Therefore, the anions in the mixed phosphates (i.e., PO_4–F, PO_3–N, PO_4–P_2O_7, and SO_4–PO_4) play different roles in optimizing the operation voltage, structural stability, and electrochemical activity of phosphate-based polyanionic cathode materials.[87] For example, F^- with a high electronegativity can powerfully enhance the energy density of fluorophosphates by further weakening the covalent properties of M–O. The crystalline structure of Na_xMPO_4F (M = Fe and Mn) exhibits great difference with $NaMPO_4$ (M = Fe and Mn). Na_2FePO_4F belongs to orthorhombic (Space group: *Pbcn*) with a [$FePO_4F$] layer comprised of PO_4 tetrahedra and face-shared dioctahedral $Fe_2O_7F_2$ and FeO_4F_2 octahedra, and this special 2D layered structure can accelerate the two Na^+ migration.[88] The theoretical capacity of Na_2FePO_4F is as high as 124 mAh g^{-1} based on the one electron redox of iron, and its two discharge plateaus are defined at 3.06 V and 2.91 V, respectively. Subsequently, Yang and co-workers confirmed the long/short-range structure evolution and the sodium-storage mechanism of Na_2FePO_4F by DFT calculation, ex situ solid-state nuclear magnetic resonance (NMR), and in situ XRD.[89] They found that the two two-phase reactions ($Na_2FePO_4F \rightarrow Na_{1.5}FePO_4F$ and $Na1_{.5}FePO_4F \rightarrow NaFePO_4F$) dominate during the (de)sodiation process according to ex situ ^{23}Na MAS NMR spectrum (**Figure 6**a). In addition, the Na^+ involved in the redox reactions only occurs on Na2 site (active), not including Na1 site (inactive), and the generated intermediate phase of $Na_{1.5}FePO_4F$ has the space group of $P2_1/C$ through DFT calculation. Unlike the 2D structure of Na_2FePO_4F, the Na_2MnPO_4F (Space group: $P2_1/C$) with 3D frame show distinctive electrochemical properties.[90] Kang and co-workers found that Na_2MnPO_4F owns an initial discharge

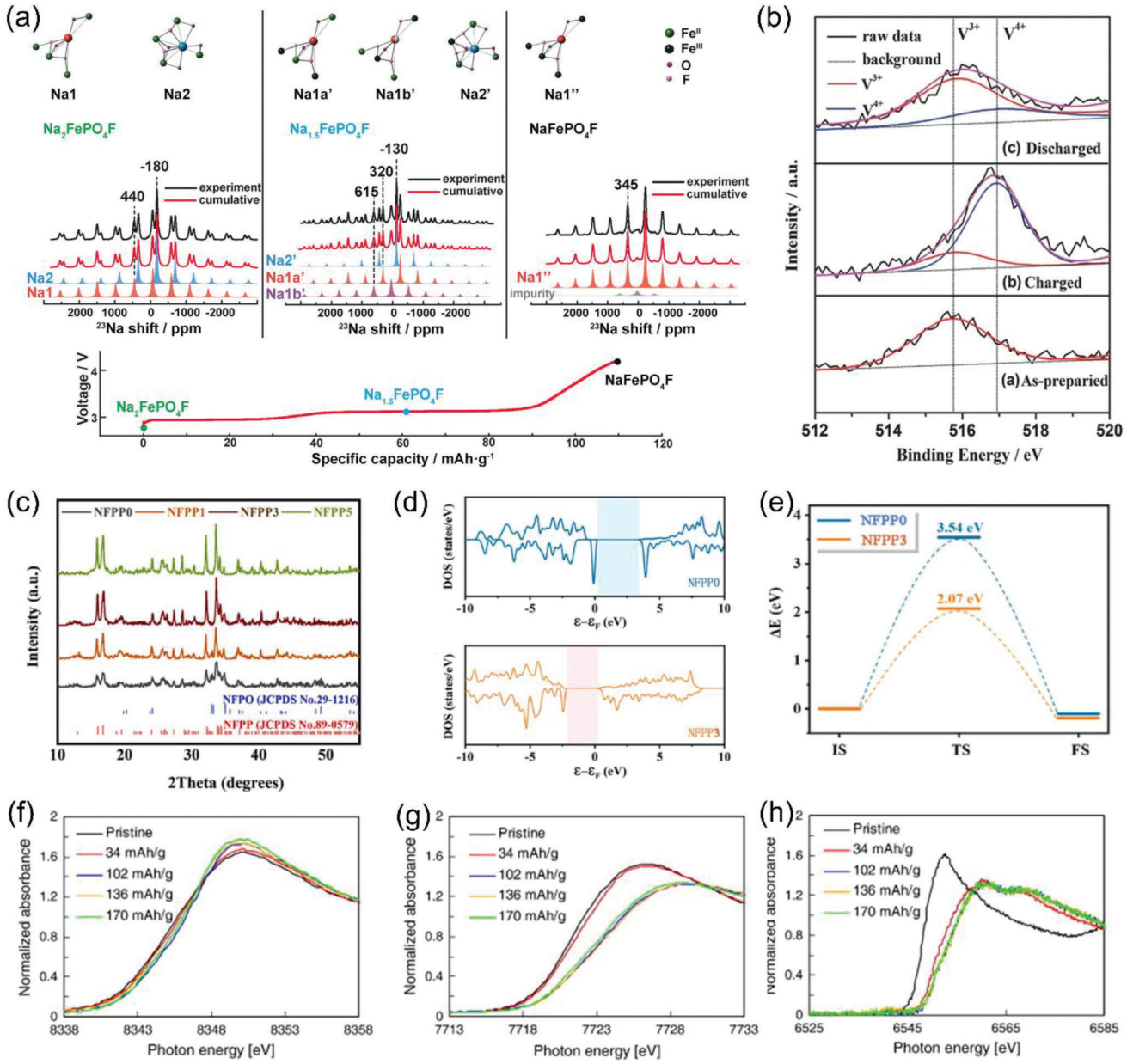

Figure 6. a) The local environment of the different Na sites and the ^{23}Na MAS NMR spectra in Na_2FePO_4F, $Na_{1.5}FePO_4F$, and $NaFePO_4F$, respectively, and the corresponding charge curve (first cycle) of Na_2FePO_4F electrode. Reproduced with permission.[89] Copyright 2018, Wiley-VCH. b) XPS spectra of $NaVPO_4F$/C electrodes at different stages. Reproduced with permission.[96] Copyright 2017, Wiley-VCH. c) The XRD patterns of $Na_4Fe_3(PO_4)_2P_2O_7$ with different Fe-defect contents. d) Density of states and e) Na^+ migration energy barriers of $Na_4Fe_{2.91}(PO_4)_2P_2O_7$ and $Na_4Fe_3(PO_4)_2P_2O_7$. Reproduced with permission.[41] Copyright 2021, Elsevier. f) Co, g) Mn, and h) Ni XANES spectra and absorption energy values at the absorbance of 0.5 obtained from pristine and charged electrodes. Reproduced with permission.[102] Copyright 2013, Elsevier.

capacity of 120 mAh g^{-1}, close to its theoretical capacity of 125 mAh g^{-1} (1 Na^+).[90] Based on DFT calculations, they revealed the extraction of the second Na^+ occurs at ≈4.67 V, which is too high resulting in the risk of electrolyte decomposition.

Sodium-vanadium fluorophosphates, widely reported as cathodes for SIBs, include $Na_3V_2(PO_4)_2F_3$, $Na_3V_2O_2(PO_4)_2F$, and $NaVPO_4F$.[91–93] Among these cathode materials, tetragonal $Na_3V_2(PO_4)_2F_3$ is the most classical cathode material and has a relatively large theoretical capacity of 128 mAh g^{-1}, accompanied by solid-solution reaction and two-phase reaction. Croguennec et al. thoroughly investigated the crystalline structure evolution of $Na_3V_2(PO_4)_2F_3$ with the electrochemical extraction of Na^+ by operando synchrotron XRD, XANES at V K edge, and ^{51}V MAS NMR.[94,95] After full desodiation, the charge disproportionation of V^{5+} and V^{3+} in $NaV_2(PO_4)_2F_3$ immediately occurs with the extraction of one Na^+. Similar to $Na_3V_2(PO_4)_2F_3$, $Na_3V_2O_2(PO_4)_2F$ with $V_2O_{10}F$ double octahedron also belongs to the tetragonal *I*4/*mmm* space group and has a slightly larger

theoretical capacity of 130 mAh g^{-1} with two distinctive charge–discharge plateaus at 3.6 and 4.0 V.[89] Hu et al. explored the sodium-storage mechanism of $Na_3V_2O_2(PO_4)_2F$ by in situ XRD, which shows obvious solid-solution process.[39] This process might be boosted by the more disordered Na^+/vacancy feature because of the Na^+/vacancy ordering of $Na_3V_2O_2(PO_4)_2F$. Compared with $Na_3V_2(PO_4)_2F_3$, the redox potential of $Na_3V_2O_2(PO_4)_2F$ reduces due to the increase in the molar ratio between O and F. $NaVPO_4F$ as another major member of sodium–vanadium fluorophosphates has been reported as the cathode for SIBs with a large theoretical capacity of 143 mA h g^{-1}. The monoclinic phase (space group: *C*2/*c*) and tetragonal phase (Space group: *I*4/*mmm*) of $NaVPO_4F$ can be obtained under different temperatures.[24] Jiao et al. utilized ex situ XPS to analyze the sodium-storage mechanism based on the valance change of V.[96] After full charge/discharge, V^{3+} and V^{4+} are always detectable (Figure 6b), suggesting the relevant redox reactions are not completely reversible and Na^+ in $NaVPO_4F$ cannot be fully extracted.

Besides, the mixed $PO_4-P_2O_7$ framework is sufficiently stable to be the sodium host in the sodium-ion compounds. Hence, the orthorhombic $Na_4M_3(PO_4)_2P_2O_7$ (M = Fe, Mn, Co, Ni, etc.) with a space group of $Pn2_1a$ is used as the cathode for SIBs, and exhibits better structural/thermal stability and high operation voltage than $NaMPO_4$ and $Na_2MP_2O_7$.[97,98] In general, the corner-shared or edge-shared MO_6 octahedra are linked by PO_4 tetrahedra to form a layer unit in the *b*-*c* plane, and the layer units are further connected by P_2O_7 along with *a*-axis to form an open 3D structure, benefitting for Na^+ migration. In 2013, Kang et al. first investigated the sodium-storage capability of $Na_4Fe_3(PO_4)_2P_2O_7$, which possesses a large reversible capacity of 113.5 mAh g^{-1} (≈88% theoretical capacity) and a high redox potential of ≈3.2 V (vs Na^+/Na) based on the Fe^{3+}/Fe^{2+} redox couple.[99] Subsequently, they discussed the relevant electrochemical mechanism and thermal stability.[31] According to the results of *ex-situ* XRD, only a single phase (solid-solution) reaction can be observed with the intercalation/extraction of Na^+, and the accompanied volumetric change is only 4%. Furthermore, combined with in situ high-temperature XRD and differential scanning calorimetry analyses, solid-solution $Na_xFe_3(PO_4)_2P_2O_7$ ($1 < x < 4$) has no clear change at temperatures as high as 530 °C, suggesting the superior thermal stability. However, the reported $Na_4Fe_3(PO_4)_2P_2O_7$ generally contains a small amount of inactive maritice $NaFePO_4$ impurities, further decreasing the reversible capacity. Thereby, Cao's group synthesized pure-phase $Na_4Fe_{2.91}(PO_4)_2P_2O_7$ with Fe vacancies using the Fe-defect strategy, as shown in Figure 6c.[41] This method can inhibit the generation of inactive maritice $NaFePO_4$, and improve the electrochemical performance of $Na_4Fe_{2.91}(PO_4)_2P_2O_7$ (110.9 mAh g^{-1} at 0.2 C, and ≈52 mAh g^{-1} at 100 C). Besides, the band gap and migration energy barriers of $Na_4Fe_{2.91}(PO_4)_2P_2O_7$ are lower than those of $Na_4Fe_3(PO_4)_2P_2O_7$, thus enhancing the electrochemical kinetics (Figure 6d,e).

Noticeably, the isostructural $Na_4M_3(PO_4)_2P_2O_7$ (M = Mn, Co, and Ni) can also be used as the cathode for SIBs. Among them, the ionic conductivity of $Na_4Mn_3(PO_4)_2P_2O_7$ at 330 °C is 2.7×10^{-5} S cm^{-1}, which is higher than those of $Na_4Co_3(PO_4)_2P_2O_7$ (1.3×10^{-6} S cm^{-1}) and $Na_4Ni_3(PO_4)_2P_2O_7$ (2.1×10^{-7} S cm^{-1}).[100] The $Na_4Mn_3(PO_4)_2P_2O_7$ as cathode materials for SIBs was first reported by Kang et al., which possesses a large energy density of 416 W h kg^{-1} with a high Mn^{3+}/Mn^{2+} redox potential of 3.84 V (vs Na^+/Na).[101] In comparison with other Mn-based cathodes, the Na^+ diffusion channels can be enlarged by the Jahn–Teller distortion of Mn^{3+} in $Na_4Mn_3(PO_4)_2P_2O_7$, rather than the common structural collapse. Meanwhile, the multiphase reaction of $Na_4Mn_3(PO_4)_2P_2O_7$ during the charge-discharge process just causes a slight volume change of ≈7%, ensuring the superior cycling stability of $Na_4Mn_3(PO_4)_2P_2O_7$. Subsequently, Nose et al. demonstrated that $Na_4Co_3(PO_4)_2P_2O_7$ as the cathode for SIBs has a large specific capacity of 95 mAh g^{-1} at a rate of 0.2 C due to 2.2 Na^+ insertion/extraction.[33] The $Na_4Co_3(PO_4)_2P_2O_7$ with multiredox couples at the potential region of 4.1–4.7 V, and the ultrahigh operation voltage is the main advantages of $Na_4Co_3(PO_4)_2P_2O_7$ cathode. In addition, the reversible capacity of $Na_4Co_3(PO_4)_2P_2O_7$ is still as high as 80 mAh g^{-1} even at the current density of 4.25 A g^{-1}, indicating fast-electrochemical kinetics. Nevertheless, the common electrolytes are prone to decomposition under so high operation voltages (4.7 V), resulting in poor cycling performance. More importantly, the high cost of Co inevitably hinders its practical application. Therefore, Nose et al. further explore the sodium-storage performance of Mn, Ni-substituted $Na_4Co_3(PO_4)_2P_2O_7$ ($Na_4Co_{2.4}Mn_{0.3}Ni_{0.3}(PO_4)_2P_2O_7$), which also shows a large initial capacity of 104 mAh g^{-1} and only has two reversible (dis)charge plateaus (4.2 V and 4.6 V, vs Na^+/Na).[102] They found that Ni, Mn, and Co all are involved in the electrochemical reaction during the (de)sodiation process through the ex situ XANES measurement (Figure 6f–h), based on the charge compensation mechanism. Similarly, $Na_4Ni_3(PO_4)_2P_2O_7$ as a cathode for SIBs also displays an ultrahigh voltage of 4.8 V, which is the highest operation voltage known at present.[103] Additionally, other types of phosphate-based mixed polyanionic cathodes have also been reported, such as $Na_3V(PO_3)_3N$,[104] $Na_3MPO_4CO_3$ (M = Fe, Mn, Co, and Ni),[105,106] and $Na_3Fe_2(SO_4)_2PO_4$.[107]

4. Strategies for the High-Performance Phosphate-Based Polyanionic Cathodes

Phosphate-based polyanionic compounds as the promising cathode candidates for SIBs have exhibited outstanding comprehensive performances, including high operation voltage, excellent structure stability, and good safety. Nevertheless, there are still many knotty problems causing certain difficulties in the practical application of phosphate-based polyanionic compounds. First of all, the isolated electronic structure of transition metal ions in phosphate-based polyanionic cathodes results in poor intrinsic conductivity, causing undesirable rate performance. Second, suffering from inactive polyanions with large molecular mass, the reversible capacities of phosphate-based polyanionic compounds still need improvement. Besides, the relatively larger and heavier Na^+ makes sluggish electrochemical kinetics and serious volume variation of cathodes, so the rate/cycling performance of phosphate-based polyanionic cathodes is unsatisfactory for their practical application. Finally, considering the ambient temperature and redox potentials of partial phosphate-based polyanionic compounds, it is difficult for the common electrolytes to stimulate the sodium-storage performance of all phosphate-based polyanionic cathodes under special conditions

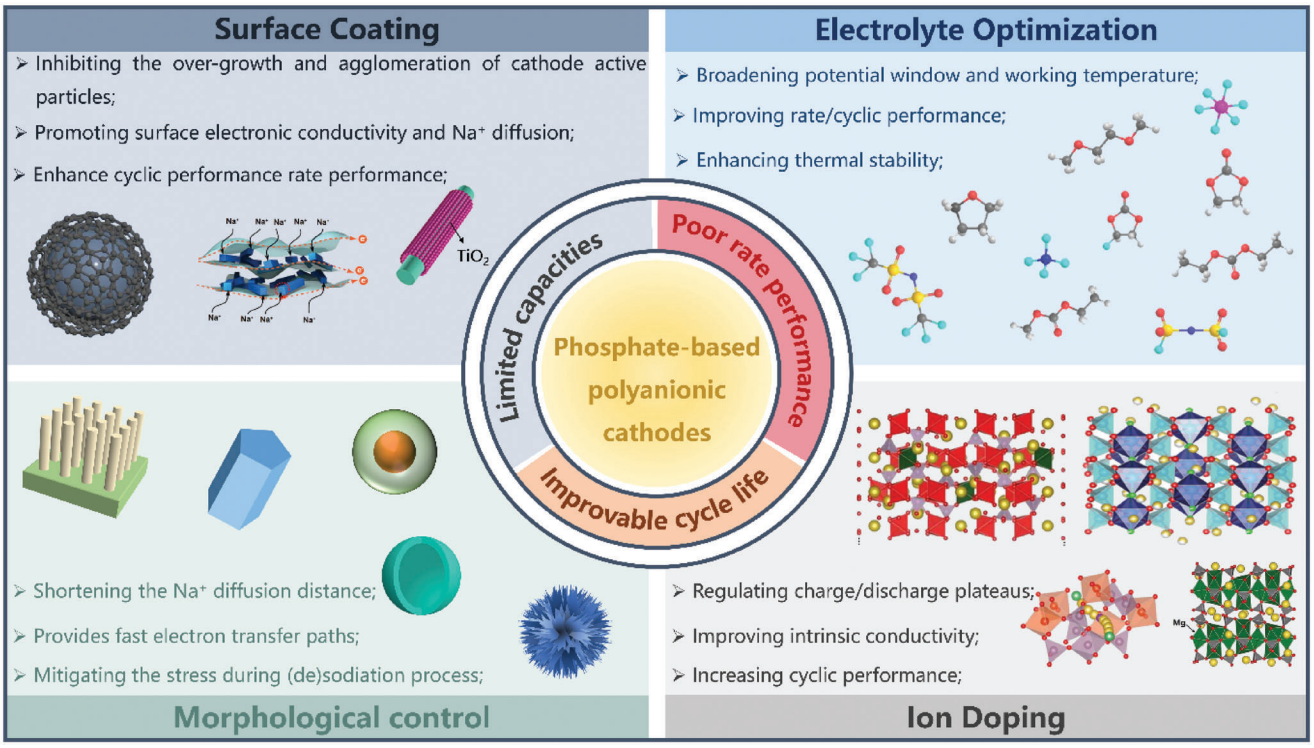

Figure 7. The issues and the corresponding optimization strategies of the phosphate-based polyanionic compounds for SIBs.

(such as extreme temperatures and high operation voltages). In response to these challenges, diverse optimization strategies have been reported for enhancing the sodium-storage performance of phosphate-based polyanionic materials, including surface coating, morphological control, ion doping, and electrolyte optimization. Herein, the issues and the corresponding optimization strategies of phosphate-based polyanionic cathodes in SIBs have been systematically summarized in **Figure 7**.

4.1. Surface Coating

Surface coating is the modification of the surface of phosphate-based polyanionic materials for improving their electrochemical properties. The common surface coating methods include carbon coating and inorganic coating (such as TiO_2 and Al_2O_3). It is noteworthy that these surface coatings have very different effects on the sodium-storage behaviors of phosphate-based polyanionic materials. For example, carbon coating can generally enhance the surface electronic conductivity and inhibit the agglomeration of cathode active materials, thus improving the rate performance and cycling stability. Komaba et al. used 2.0 wt% ascorbic acid as a carbon source to synthesize Na_2FePO_4F/C composite.[108] Compared with pure Na_2FePO_4F, the reversible capacity of Na_2FePO_4F/C is much larger (110 mAh g^{-1} at 6.2 mA g^{-1}) profiting from its good electrical conductivity and the relatively small particle size (30–200 nm). Similarly, Hu's group also prepared the carbon-coated $Na_3V_2(PO_4)_3$ taking advantage of sugar as the carbon source, and the carbon layer in this composite is 9.4 wt% with a thickness of ≈6 nm.[109] However, its reversible capacity is only 25 mAh g^{-1} at 1 C due to the imperfect carbon matrix and large particle size of $Na_3V_2(PO_4)_3$. To further improve the rate performance of $Na_3V_2(PO_4)_3$, Yu's group prepared a 3D hierarchical meso- and microporous $Na_3V_2(PO_4)_3$@reduced graphene oxide ($Na_3V_2(PO_4)_3$@rGO, **Figure 8**a,b), which delivers a large specific capacity of 112 mAh g^{-1} at 1 C and superior rate performance of 86 mAh g^{-1} at 100 C (Figure 8c).[110] Subsequently, Mai et al. also utilized rGO as the carbon source and designed a layer-by-layer $Na_3V_2(PO_4)_3$@rGO through the hydrothermal method.[111] The as-prepared $Na_3V_2(PO_4)_3$@rGO achieves an outstanding sodium-storage performance (a specific capacity of 118 mA h g^{-1} at 0.5 C; a capacity retention of 70% after 15 000 cycles at 50 C).

According to these researches, the significant improvement in the electrochemical performance of $Na_3V_2(PO_4)_3$ can be attributed to the special composite structure (3D porous structure or layer-by-layer structure), uniform distribution of nano-$Na_3V_2(PO_4)_3$, and the intimate wrapping of highly conductive rGO. Nevertheless, the high-cost rGO is contrary to the main superiority of low-cost SIBs, so some novel carbon matrices are developed, such as carbon fiber, multiwalled CNT (MWCNT), and carbon sheet. For instance, Jiao et al. designed $NaVPO_4F$/carbon nanofibers as the cathode for SIBs by an electrospinning technique (Figure 8d), and the ultrafine $NaVPO_4F$ particles (≈6 nm) are evenly embedded into the porous carbon nanofiber (Figure 8e).[96] The nanosized particles and porous structure of carbon nanofiber can enhance the electronic conductivity and alleviate the volume changes during (de)sodiation process. As a result, the $NaVPO_4F$/carbon nanofibers show a remarkable rate performance (61.2 mA h g^{-1} at 50 C) and long

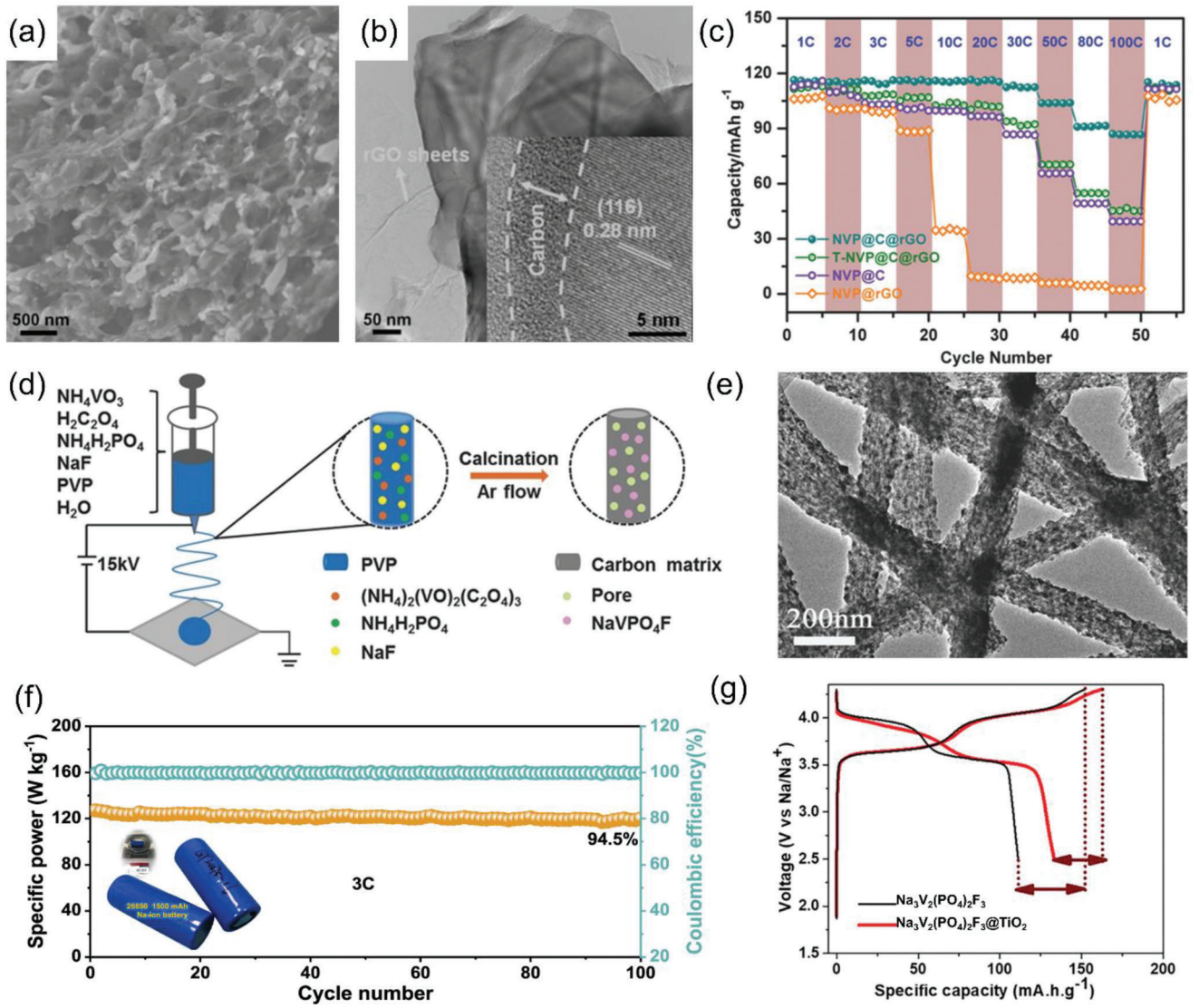

Figure 8. a) Scanning electron microscopy (SEM) image, b) HRTEM image, and c) rate performance of the 3D hierarchical porous $Na_3V_2(PO_4)_3$@rGO. Reproduced with permission.[110] Copyright 2015, Wiley-VCH. d) Schematic illustration of the formation process and e) TEM image of $NaVPO_4F$/carbon nanofibers. Reproduced with permission.[96] Copyright 2017, Wiley-VCH. f) Cycling performance of 26 650 cells of $Na_3(VOPO_4)_2F$/C at 3 C, and the inserts are the photograph of 26 650 prototype cells. Reproduced with permission.[114] Copyright 2021, Springer Nature. g) First cycle of pure $Na_3V_2(PO_4)_2F_3$ and $Na_3V_2(PO_4)_2F_3$@TiO_2. Reproduced with permission.[120] Copyright 2021, Wiley-VCH.

cycle life (capacity retention of 96.5% after 1000 cycles at 2 C). Similarly, Fan and co-workers also prepared binder-free maricite $NaFePO_4$ (≈1.6 nm)/porous carbon fiber cathode for boosting the electrochemical performance.[112] The reversible capacity can reach 145 and 61 mA h g^{-1} at 0.2 and 50 C, respectively, and its capacity retention maintains 89% after 6300 cycles. Furthermore, Cao et al. prepared a nanosized $Na_4Fe_3(PO_4)_2P_2O_7$ spheres growing on MWCNT by surface modification and spray drying, and this composite exhibits a superior electrochemical performance (115.7 mA h g^{-1} at 0.1 C and 95% capacity retention after 1200 cycles at 2 C).[113] The scaled synthesis of $Na_3(VOPO_4)_2F$/C (2 kg) by a facile high-energy ball milling method was reported by Hu's group, which exhibits a specific capacity of 142 mAh g^{-1} at 0.1 C.[114] More importantly, the 26 650 prototypes (vs HC anode) deliver a superior cycling performance (Figure 8f), suggesting good business prospects. In addition, other common phosphate-based polyanionic cathodes ($Na_2FeP_2O_7$, Na_2FePO_4F, $Na_7V_3(P_2O_7)_4$, $Na_4MnV(PO_4)_3$, etc.) have also been modified by MWCNT, carbon sheet, or carbon nanofiber and realized remarkable electrochemical performance.[115–118] Although these carbon matrices greatly enhance the sodium-storage capability of phosphate-based polyanionic cathodes, the excessive carbon is detrimental to the energy density of SIBs.

Apart from carbon coating, inorganic coating is the other effective coating strategy to enhance sodium-storage performance. In general, the atomic layer deposition (ALD) technique can ensure a uniform inorganic coating on the surface of phosphate-based polyanionic cathodes. Based on this technique, Li and

co-workers found the generation of Al_2O_3 layer on the surface of $Na_3V_2(PO_4)_3$ is greatly beneficial for the improvement of rate performance.[119] This is because the deposited Al_2O_3 coating has a superior ionic conductivity. Similarly, Mukherjee et al. prepared $Na_3V_2(PO_4)_2F_3$ with ultrathin amorphous TiO_2 layer (≈2 nm), and $Na_3V_2(PO_4)_2F_3$@TiO_2 has a larger capacity than bare $Na_3V_2(PO_4)_2F_3$, as shown in Figure 8g.[120] This can be attributed to the construction of TiO_2 coating, which can facilitate the migration of Na^+ through the cathode–electrolyte interphase (CEI) layer, leading to the rapid sodium-storage kinetics. Besides, the reversible capacity of $Na_3V_2(PO_4)_2F_3$@TiO_2 is still as high as 107 mAh g^{-1} (>16% improvement of bare $Na_3V_2(PO_4)_2F_3$) after 200 cycles, since the TiO_2 layer can alleviate the volume expansion of cathode and the decomposition of the electrolyte. Differing from the ALD method, Wang et al. also achieved the uniform coating of the RuO_2 layer on $Na_3V_2(PO_4)_2F_3$ nanowire through the hydrothermal method, and the related specific capacity can maintain 90 mAh g^{-1} even at 20 C.[121] They revealed the RuO_2 coating with high conductivity can selectively grow in the (002) direction of $Na_3V_2(PO_4)_2F_3$, which reduces the Na^+-diffusion energy barriers on the *ab* plane, leading to the remarkable rate performance. In brief, the coating layer on the surface of the cathode material can prevent Na^+ from escaping and the cathode material from reacting with the air and electrolyte. Meanwhile, the coating layer is preferentially a conductive material with good electrical/ionic conductivity, which can improve the conductivities of the cathode materials and enhance the electrochemical properties.

4.2. Morphological Control

In general, downsizing phosphate particles to the nanoscale can shorten the pathways of Na^+ diffusion, which is conducive to rapid electrochemical kinetics. Meanwhile, the nanosized phosphate-based polyanionic compounds are suitable for adjusting the volume changes during the continuous (de)sodiation process, thus preventing the pulverization of cathode materials and increasing the cycle life. More importantly, the relatively large specific surface area of nanosized phosphates with special morphologies is curial to boost the interfacial Faradaic reactions in the batteries and the Na^+ flux across the electrode–electrolyte interface, leading to the increase in reversible capacity.[122] Hence, the nanostructure processing shows a great influence on the sodium-storage behavior of phosphate-based polyanionic cathodes. In recent years, the hydrothermal/solvothermal method is one of the most popular synthesis routes to prepare nanosized phosphates.[123,124] For instance, Karthik et al. utilized the hydrothermal method to prepare nanosized $NaFePO_4$ with an average particle size of 70–90 nm, which delivers a larger specific capacity (90 mAh g^{-1} at 0.1 C) than bulk $NaFePO_4$.[125] The effect of morphologies on the electrochemical performance of Na_2FePO_4F/C composites was investigated by Sun and co-workers.[126] The double-shelled hollow spheres exhibit the best electrochemical performance (a high reversible capacity of 120.1 mAh g^{-1} at 0.1 C, a capacity retention of 92.5% after 200 cycles). This result indicates the importance of morphological control for sodium-storage properties. In addition, Qi et al. revealed that the regulation of pH value is also necessary to design some nanostructure cathodes through the hydrothermal method.[127] As shown in **Figure 9**a,b, $Na_3(VPO_4)_2F_3$ nanoflowers were obtained under a weak acid environment, and the reversible capacity can maintain 99.2 mAh g^{-1} at 0.2 C after 500 cycles with a high average voltage of ≈3.76 V.

Although the hydrothermal/solvothermal method is a facile way to control the morphologies, its low yield and long reaction time make it hard to achieve large-scale production. Therefore, sol–gel and coprecipitation methods with good maneuverability and controllability are also widely reported for gaining phosphate-based polyanionic materials with special structures. Lai and co-workers developed a triclinic off-stoichiometric $Na_{3.12}Mn_{2.44}(P_2O_7)_2$/C with a hierarchical porous structure by sol–gel method and carbothermal reduction process.[78] The nanosized cathode active material of $Na_{3.12}Mn_{2.44}(P_2O_7)_2$ embedded into the porous carbon matrix delivers a prolonged cycle life (75% capacity retention at 5 C after 500 cycles) and superb energy density (376 Wh kg^{-1}). Similarly, Chou et al. prepared a 3D porous frame-supported $Na_3V_2(PO_4)_3$/C, which shows excellent rate performance (76.9% capacity retention at 192 C vs its initial capacity of 98.6 mAh g^{-1} at 0.5 C) and ultralong cycle life (91.4% capacity retention at 10 C after 2000 cycles), much better than the electrochemical performance of bulk $Na_3V_2(PO_4)_3$.[128] Thereby, the conductive interconnected network and full contact between cathode and electrolyte are beneficial for boosting the sodium-storage performance. The scalable room-temperature synthesis of multishelled $Na_3(VOPO_4)_2F$ microspheres using a facile and rapid coprecipitation strategy was reported by Hu's group, which effectively decreases the production cost of cathode materials with special morphologies.[39] The as-prepared $Na_3(VOPO_4)_2F$ microspheres display a large specific capacity of 111 mAh g^{-1} at 0.1 C and a high capacity retention of 70% at 15 C even after 3000 cycles. In comparison with other reported bulk $Na_3(VOPO_4)_2F$, the electrochemical performance of pure $Na_3(VOPO_4)_2F$ microspheres is much better. Subsequently, they synthesized $Na_3(VOPO_4)_2F$ nanocubes through a similar coprecipitation strategy at the pH of 6.[40] Its yield and capacity retention over 8000 cycles at 25 C can reach 99.1% and 72%, respectively, suggesting a remarkable potential of commercial application of this coprecipitation strategy. These works prove the importance of morphology design (microsphere vs nanocube), and the nanosized active particles exhibit better sodium-storage performance than their bulk counterparts.

Spray drying as another universal synthetic method is utilized to prepare cathode materials with spherical morphologies (i.e., hollow spheres and solid spheres), which can also achieve hybridization with high conductive materials (i.e., 3D graphene, CNT, and rGO).[58,92,129] Noticeably, all the composites prepared by spray drying (i.e., $Na_4Fe_3(PO_4)_2P_2O_7$/3D graphene, hollow Na_2MnPO_4F/C spheres, and $Na_4Mn_2Co(PO_4)_2P_2O_7$/CNT, Figure 9c) show excellent sodium-storage performance.[130–132] However, the relatively complex equipment, high energy consumption, and low efficiency of spray drying hinder its development in SIBs. Moreover, other common synthesis routes, such as the template method and electrospinning, can also prepare phosphate-based polyanionic cathodes with special morphologies and remarkable electrochemical performance. For example, Qiao and co-workers designed a single crystalline $Na_3V_2(PO_4)_3$ with a porous structure using polymer-stabilized droplet

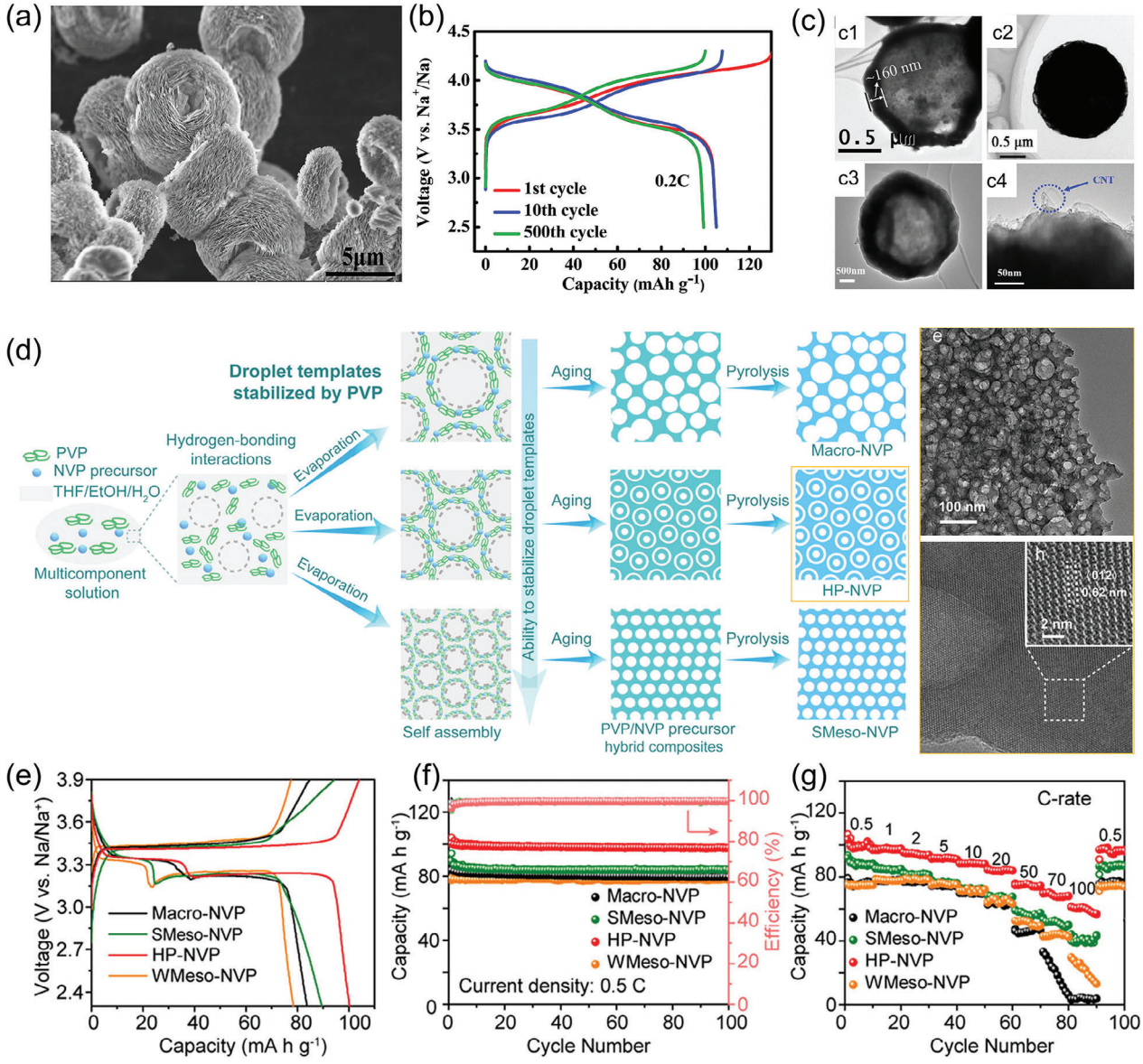

Figure 9. a) SEM image and b) the cycling performance of $Na_3(VPO_4)_2F_3$ nanoflowers. Reproduced with permission.[127] Copyright 2016, The Royal Society of Chemistry. c) SEM images of spherical phosphate-based polyanionic cathodes prepared by spraying drying (c1: Na_2MnPO_4F/C hollow spheres, c2: $Na_4Fe_3(PO_4)_2P_2O_7$@3D graphene, and c3/c4: $Na_4Mn_2Co(PO_4)_2(P_2O_7)$/C-CNT spheres). c1) Reproduced with permission.[130] Copyright 2017, Elsevier. c2) Reproduced with permission.[131] Copyright 2018, Elsevier. c3-c4) Reproduced with permission.[132] Copyright 2019, American Chemical Society. d) Tentative formation mechanism of porous single crystalline $Na_3V_2(PO_4)_3$ through polymer stabilized droplet template method, and TEM images of hierarchically meso/macropores $Na_3V_2(PO_4)_3$. e) Initial charge/discharge curves, f) cycling performance, and g) rate performances of porous single crystalline $Na_3V_2(PO_4)_3$. Reproduced with permission.[133] Copyright 2021, Wiley-VCH.

template method (Figure 9d).[133] The generated porous single-crystal structure can greatly shorten the Na^+ diffusion distance and facilitate ion transition, leading to excellent electrochemical properties (100 mA h g^{-1} at 0.5 C, and 81 mA h g^{-1} at 1 C after 10 000 cycles). Meanwhile, they demonstrated the pore structure, pore size, and specific surface area of porous single crystalline $Na_3V_2(PO_4)_3$ have a significant effect on the sodium-storage performance (Figure 9e–g). Based on the above-mentioned discussion, morphological control is beneficial for improving the electrochemical performance, but the low tap density and complex preparation process are the bottleneck in the practical application.

4.3. Ion Doping

Ion doping can enhance the sodium-storage performance by stabilizing the crystal structures or modifying the conductivity of phosphate-based polyanionic cathodes, and has been widely applied for reducing cost, enhancing cycling performance, regulat-

Table 1. Effects of ion doping strategy on the performance of phosphate-based polyanionic compounds for SIBs.

Doping element		Effects
Cation doping	Inactive metal ion doping (Li^+, K^+, Mg^{2+}, Al^{3+}, Cr^{3+}, Ca^{2+}, etc.)	• Suppress the lattice distortion; • Reduce internal resistance; • Enhance crystalline structure stability; • Enhance the ionic conductivity; • Enlarge interlayer space
	Active metal ion doping (Mn^{2+}, Fe^{2+}, Ni^{2+}, Co^{2+}, etc.)	• Increase the specific capacity; • Enhance the ionic conductivity; • Enhance crystalline structure stability; • Improve the electrochemical reaction kinetics;
Anion doping	Simple anion doping (F^-, Cl^-, etc.)	• Increase the specific capacity; • Improve the electrochemical reaction kinetics;
	Polyanion doping (BO_4^{4-}, SiO_4^{5-}, etc.)	• Increase the specific capacity; • Enhance crystalline structure stability; • Improve the electrochemical reaction kinetics

ing redox potential, or improving intrinsic conductivity.[134] In general, ion doping can be divided into cation doping and anion doping. Noticeably, the types of ion dopants exhibit different effects on the optimization of electrochemical performance (**Table 1**).[135–137] Among them, cation doping is mainly aimed at active transition metal sites at octahedra and interstitial Na^+ sites, and the commonly used dopants consist of Al, Mg, Fe, Mn, Mo, Co, Cr, K, Li, etc. For instance, Wang et al. reported the Al-doped $Na_4Co_3(PO_4)_2P_2O_7$ ($Na_{3.85}Co_{2.85}Al_{0.15}(PO_4)_2P_2O_7$), which shows better rate performance and longer cycle life than pure $Na_4Co_3(PO_4)_2P_2O_7$, suggesting the positive effect of Al doping on the electrochemical kinetics and structural stability.[138] This is because the charge transfer resistance of $Na_{3.85}Co_{2.85}Al_{0.15}(PO_4)_2P_2O_7$ is much smaller than that of $Na_4Co_3(PO_4)_2P_2O_7$ (49.5 Ω vs 120.6 Ω). Moreover, Lu et al. also found Mg-doped $Na_2FeP_2O_7$ cathode exhibits better electrochemical performance than bulk $Na_2FeP_2O_7$.[139] The experimental results and DFT calculation disclosed that the 5% Mg doping can increase the electronic conductivity of $Na_2FeP_2O_7$ due to the existence of bandgap and obtains a specific capacity of 90 mAh g^{-1} at 0.1 C without obvious degradation after 40 cycles. Interestingly, the massive Mg doping of 20% does not cause devastating damage to the electrochemical properties of $Na_2FeP_2O_7$, just a slight decrease in reversible capacity. For $Na_3V_2(PO_4)_3$, the metal doping (such as Mg, Al, Cr, and Fe) not only improves conductivity and enhances structural stability of $Na_3V_2(PO_4)_3$, but also can inspire the V^{5+}/V^{4+} redox couple for increasing the sodium-storage capability. Okada's group first found Mg-doped $Na_3V_2(PO_4)_3$ ($Na_{3.2}V_{1.8}Mg_{0.2}(PO_4)_3$) has a larger reversible capacity than pure $Na_3V_2(PO_4)_3$ due to the partial utilization of high-voltage V^{5+}/V^{4+} redox couple.[140] They proposed that the Mg^{2+} occupies the V site leading to the introduction of extra active Na^+ for charge compensation. Nevertheless, the specific capacity of $Na_{3.5}V_{1.5}Mg_{0.5}(PO_4)_3$ decreases owing to the irreversible redox reaction of V^{5+}/V^{4+} in this Mg-rich phase. As shown in **Figure 10**a, most Mg^{2+} are distributed on the particle surface, while less Mg^{2+} are dispersed in the bulk of $Na_3V_2(PO_4)_3$ particle, the nonuniform distribution of Mg doping results in a faster diffusion of Na^+ on the surface than in the particles.[141] Therefore, Wu and co-workers demonstrated that Mg-doped $Na_3V_{2-x}Mg_x(PO_4)_3$/C composite shows more remarkable rate performance and cyclic stability than pure $Na_3V_2(PO_4)_3$.[142] Similarly, Zhao et al. found Al-doping strategy can enhance the electrochemical performance of $Na_3V_2(PO_4)_3$, and the redox peaks of V^{5+}/V^{4+} are also checked at 3.95 V.[143] According to the DFT calculation, $Na_3V_{2-x}Al_x(PO_4)_3$ shows smaller bandgap and Na^+ migration energy barrier than $Na_3V_2(PO_4)_3$, suggesting the improvement of electronic/ionic conductivity. However, excessive Al doping causes an increase in migration energy, so it is necessary to optimize the Al doping amount for achieve an excellent rate performance. To achieve the reversible three-electron redox reactions of $Na_3V_2(PO_4)_3$ ($V^{5+} \leftrightarrow V^{2+}$), Goodenough et al. synthesized Cr-doped $Na_3V_2(PO_4)_3$ ($Na_3V_{1.5}Cr_{0.5}(PO_4)_3$) with the reversible redox reactions ($V^{2+} \leftrightarrow V^{3+} \leftrightarrow V^{4+} \leftrightarrow V^{5+}$) during the voltage range of 1.0–4.4 V (Figure 10b,c).[144] The $Na_3V_{1.5}Cr_{0.5}(PO_4)_3$ exhibits a high capacity retention of 96% even after 400 cycles, indicating remarkable reversibility during the repeated Na^+ (de)intercalation. Subsequently, Chen et al. comprehensively explored the sodium-storage mechanism of $Na_3V_{1.5}Cr_{0.5}(PO_4)_3$ through theoretical calculation and various advanced characterization methods (Figure 10d,e).[145] They found that the $Na_3V_{1.5}Cr_{0.5}(PO_4)_3$ has a lower Na^+-migration energy barrier in comparison with undoped $Na_3V_2(PO_4)_3$. Meanwhile, the electrochemically inactive dopant of Cr at low voltage can reduce the forbidden bandgap, and its unpaired electron in the 3d orbital is an important factor in triggering the high-voltage redox reaction of V^{5+}/V^{4+}. Thereby, $Na_3V_{1.5}Cr_{0.5}(PO_4)_3$ has superior ionic conductivity and high operation voltage. In addition, low-cost and nontoxic transition ions (i.e., Fe, Mn, and Ti) can also stimulate the V^{5+}/V^{4+} redox couple by the partial substitution of V in $Na_3V_2(PO_4)_3$, and both reversible capacity and cycling performance are better than its pure phase.[146–148] Recently, Hu's group took low-cost Fe doping to activate the V^{5+}/V^{4+} redox and demonstrated that enough Na2 content in V-based compounds is the requirement for the activation of V^{5+}/V^{4+} redox.[149]

In the latest research, the high-entropy doping strategy is gradually becoming popular for polyanionic compounds due to the excellent electrochemical activity and structural

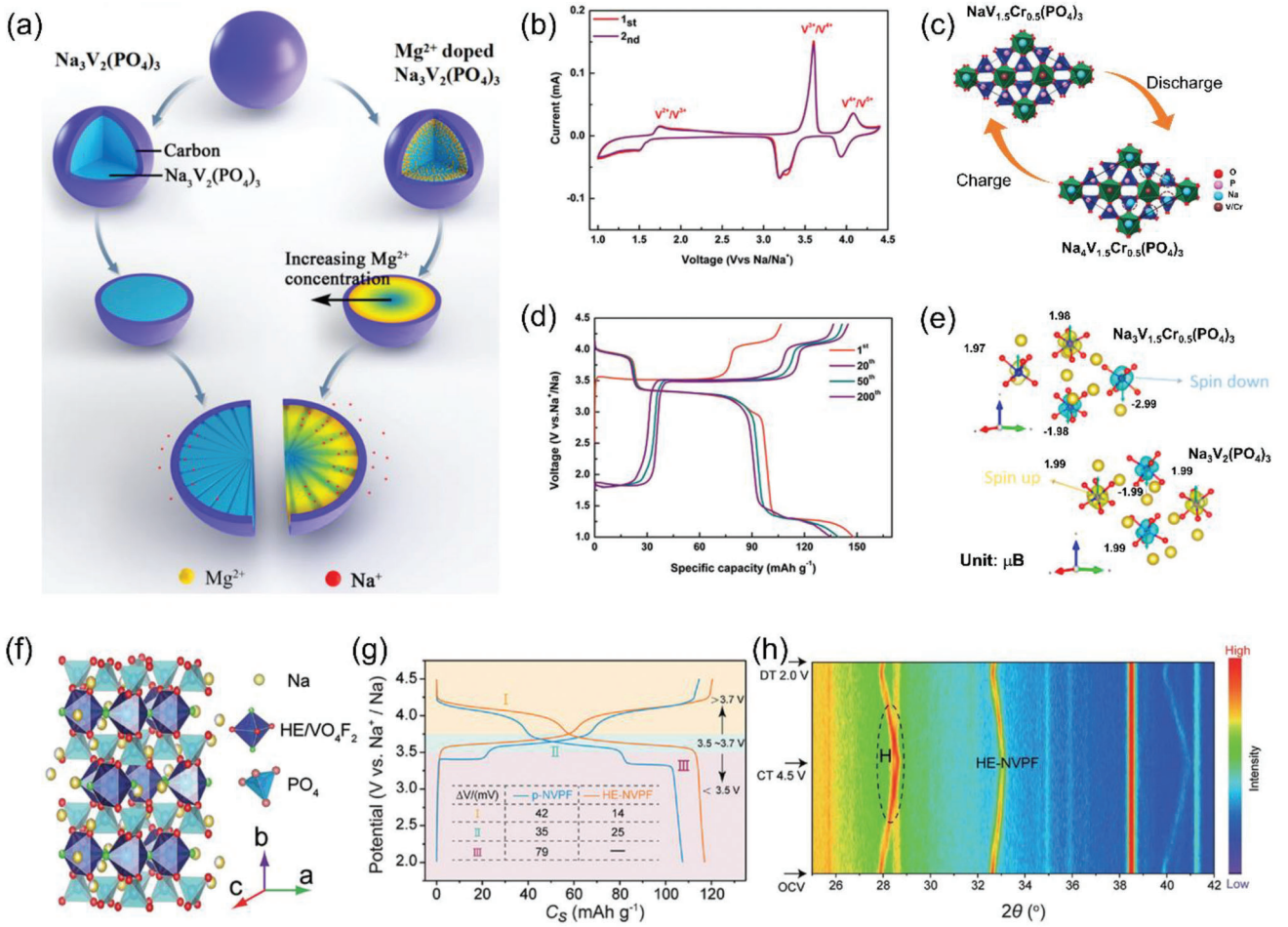

Figure 10. a) Schematic illustration of Na^+ diffusion channel in undoped or Mg^{2+}-doped $Na_3V_2(PO_4)_3$/C. Reproduced with permission.[141] Copyright 2018, American Chemical Society. b) CV profiles of $Na_3V_{1.5}Cr_{0.5}(PO_4)_3$ at 0.5 mV s^{-1} in the range of 1.0–4.4 V. c) Schematic illustration of the three-electron reaction of $Na_3V_{1.5}Cr_{0.5}(PO_4)_3$. Reproduced with permission.[144] Copyright 2020, Wiley-VCH. d) Charge–discharge curves at different rates for the $Na_3V_{1.5}Cr_{0.5}(PO_4)_3$ electrode. e) The comparative electronic spin states for $Na_3V_2(PO_4)_3$ and $Na_3V_{1.5}Cr_{0.5}(PO_4)_3$. Reproduced with permission.[145] Copyright 2021, American Chemical Society. f) Schematic illustration for the change of crystal structure of $Na_3V_{1.9}(Ca,Mg,Al,Cr,Mn)_{0.1}(PO_4)_2F_3$. g) Charge–discharge curves of $Na_3V_{1.9}(Ca,Mg,Al,Cr,Mn)_{0.1}(PO_4)_2F_3$ and pure $Na_3V_2(PO_4)_2F_3$ at 0.1 C in the potential windows of 2.0–4.3 V (vs Na^+/Na). h) In situ XRD patterns of $Na_3V_{1.9}(Ca,Mg,Al,Cr,Mn)_{0.1}(PO_4)_2F_3$ electrode in the voltage window of 2.0–4.5 V. Reproduced with permission.[151] Copyright 2022, Wiley-VCH.

stability of high-entropy dopants.[135,150] For example, Wu's group reported an advanced high-entropy fluorophosphate cathode of $Na_3V_{1.9}(Ca,Mg,Al,Cr,Mn)_{0.1}(PO_4)_2F_3$, which delivers a high energy density (445.5 Wh kg^{-1}) and a better sodium-storage performance than pure $Na_3V_2(PO_4)_2F_3$ (Figure 10f,g).[151] Figure 10h suggests that the introduction of high-entropy alloy is conducive to rearranging the disordered Na^+ at Na2 sites, inhibiting the undesirable sodium-storage behaviors at low voltage. Hence, the energy density of $Na_3V_2(PO_4)_2F_3$ can be increased to a certain degree owing to the high operating voltage. Not all metal-ion doping, however, can improve the electrochemical properties of polyanionic cathodes. Komaba et al. clarified the Mn-substituted Na_2FePO_4F ($Na_2Fe_{1-x}Mn_xPO_4F$) shows worse electrochemical activity than Na_2FePO_4F.[152] It is worth noting that $Na_2Fe_{1-x}Mn_xPO_4F$ has different crystalline structures with different molar ratios between Fe and Mn, and the crystalline structures can be divided into the layered structure ($x < 0.1$) and 3D channel structure ($0.3 < x < 1$).

For the doping at Na sites, the Li^+/K^+ can act as pillars in the framework structure to effectively improve the cycle stability by inhibiting the structural changes and suppressing undesirable phase transformations during the (de)sodiation process. The unique effects of pillar ions on the electrochemical performance and structural stability of the electrode materials have been well investigated. For example, Xia's group prepared K-doped $Na_3Fe_2(PO_4)_3$ via solid-state reaction method, the $K_{0.24}Na_{2.76}Fe_2(PO_4)_3$ shows the best sodium-storage capacity (101.3 mAh g^{-1} at 10 mA g^{-1}; 93.7 mAh g^{-1} after 500 cycles at 100 mA g^{-1}).[153] In comparison with pure $Na_3Fe_2(PO_4)_3$, the value of Na^+ diffusion coefficients for $K_{0.24}Na_{2.76}Fe_2(PO_4)_3$ is much higher (3.98×10^{-10} cm^2 S^{-1} vs 3.81×10^{-11} cm^2 S^{-1}) due to the larger lattice space. To explore the effects

of K-doping on the crystal structure, electrochemical kinetics, and sodium-storage performance, Zhang et al. then analyzed K-doped $Na_3V_2(PO_4)_2F_3$ through experiments and theoretical calculations.[154] The $Na_{2.90}K_{0.10}V_2(PO_4)_3F_3$ exhibits the most excellent electrochemical performance (120.8 mAh g^{-1} at 0.1 C, 66 mAh g^{-1} at 30 C, and a capacity retention of 97.5% at 1 C after 500 cycles). The bandgap of $Na_3V_2(PO_4)_2F_3$ reduces from 2.75 to 2.68 eV after K doping, and Na^+ ion migration barriers of $Na_3V_2(PO_4)_2F_3$ and K-doped $Na_3V_2(PO_4)_2F_3$ are 187 and 128 meV, respectively. Hence, the K-doping at Na sites is beneficial for improving ionic/electronic conductivity. What's more, Zheng et al. found Li^+ doping can achieve more than two Na^+ extraction/insertion of $Na_3V_2(PO_4)_3$, so the reversible capacity of Li-doped $Na_3V_2(PO_4)_3$ ($Na_{3-x}Li_xV_2(PO_4)_3$) is as high as ≈130 mAh g^{-1} at 0.5 C, exceeding theoretical capacity.[155] Through Rietveld refinement, nuclear magnetic resonance spectroscopy, and DFT calculation, Li^+ occupies Na2 sites with a relatively low Li amount ($x \leq 0.1$), and then occupies Na1 and Na2 sites with a high Li amount ($x > 0.1$). In addition, the rearrangement of the Li^+/Na^+ in the Na sites can activate the Na^+ at the M1 sites to enhance the sodium-storage capability.

Anion doping strategy has also exhibited huge potential to improve the electrochemical performance of phosphate-based polyanionic compounds through optimizing the ionic/electronic conductivity and crystalline structure stability. Among the various anions, F^- doping is one of the most popular anion-doping strategies. Differing from F-based phosphates, the introduction of less F^- has no significant effect on the average operation voltage, but improves electrochemical performance by optimizing the physicochemical characteristics, such as crystalline structural stability and ionic/electronic conductivity. For example, Sun and co-workers demonstrated that F-doped $Na_3V_2(PO_4)_3$ ($Na_3V_2(PO_4)_{2.93}F_{0.07}$) shows higher ionic conductivity than pure $Na_3V_2(PO_4)_3$, thus the reversible capacity of $Na_3V_2(PO_4)_{2.93}F_{0.07}$ can still reach 97.8 mAh g^{-1} at the current density of 200 mA g^{-1}.[156] In addition, some polyanions (i.e., SiO_4^{4-} and BO_4^{5-}) can also be doped into $Na_3V_2(PO_4)_3$ cathode. A series of $Na_{3+x}V_2(PO4)_{3-x}(SiO_4)_x$ has been reported by Lavela et al.[157] They found that the structural deformation and/or amorphous impurities occur after the introduction of too much SiO_4^{4-}, resulting in deterioration of the electrochemical properties. Besides, Cui et al. found that the rate performance of $Na_3V_2(PO_4)_3$ can be improved by the partial substitution of BO_4^{5-} into PO_4^{3-}.[158] This is since the band gap of the $Na_3V_2P_{3-1/6}B_{1/6}O_{12}$ is significantly narrower than that of pure $Na_3V_2(PO_4)_3$ (1.633 eV vs 2.57 eV). Subsequently, Wang et al. investigated the influence of BO_4^{5-} on the stability and electrochemical behavior of $Na_3V_2(PO_4)_3$ by the first principles.[159] According to their simulation results, B doping can considerably increase the structural stability of $Na_3V_2(PO_4)_3$ and shrink its lattice size to some extent. Recently, both Cai et al. and Zhao et al. demonstrated the strategy of simultaneous cation and anion doping to design high-capacity and long-cycle-life $Na_3V_2(PO_4)_3$-based cathodes, respectively.[160,161] Specifically, the polyanion doping aims to increase the reversible capacity by replacing PO_4^{3-}, while the introduced cations as the pillar ions are to stabilize the crystalline structure and improve the reversibility of the $Na_3V_2(PO_4)_3$ cathode. In summary, the doped ions not only can be a supporting matrix in the main crystalline structure to suppress lattice collapse and strengthen the structural stability, but also improve the electrochemical kinetics and capacity. Simultaneously, it is essential to ensure the ion dopants are positive for the electrochemical performance of cathodes, containing types and amounts.

4.4. Electrolyte Optimization

The electrolyte as the bridge between the anode and cathode shows a significant influence on safety and sodium-storage capability. Considering the unique feature of polyanionic cathodes over other types of cathodes, namely high redox potential, the strong antioxidant capacity of electrolytes becomes increasingly important for averting the decomposition of electrolytes under high voltage. Furthermore, the CEI layer formed by the decomposition of electrolytes plays a crucial role in protecting cathode materials, reducing the dissolution of metal ions, enhancing Na^+ migration, and improving the electrochemical performance at high voltage. Therefore, electrolyte optimization is an effective strategy to promote the sodium-storage performance of phosphate-based polyanionic materials. Taking the electrochemical performance of $Na_3V_2(PO_4)_3$/C at room temperature as the yardstick, Hu et al. roughly investigated the effect of sodium salt and carbonate-ester solvent.[52] Compared with $NaPF_6$, $NaBF_4$, and $NaClO_4$, $Na_3V_2(PO_4)_3$/C exhibits a higher coulombic efficiency, larger specific capacity, and more stable cycling property in the sodium bis(fluorosulfonyl) imides (NaFSI)-based electrolytes (NaFSI/ethylene carbonate (EC) + diethyl carbonate (DEC) and NaFSI/propylene carbonate (PC)) due to the less electrolyte decomposition and side reactions. In addition, the electrolyte additive of fluoroethylene carbonate (FEC) is beneficial for enhancing the stability of the CEI layer. Kucinskis et al. measured the electrochemical performance of $Na_2FeP_2O_7$/C in the electrolyte of 1 M $NaClO_4$/PC+FEC (5 wt%), and its reversible capacity can maintain 81 mAh g^{-1} at 1 C even after 500 cycles (**Figure 11**a).[162] Nevertheless, the corresponding capacity retention is only 37% in the electrolyte without the additive of FEC, revealing the necessity of using CEI-stabilizing additives.

Apart from the carbonate-ester electrolyte, the ether-based electrolyte is also used to enhance the rate performance of polyanionic cathodes based on its low viscosity and good wettability. In addition, the generated CEI layer also shows excellent structural characteristics, such as good compactness and thin layer. Ahn and co-works utilized 1 M $NaPF_6$ in 1,2-dimethoxyethane as the electrolyte to modify the electrochemical performance of $Na_3V_2(PO_4)_3$, which shows a relatively large specific capacity of 44 mAh g^{-1} even at 854 C and a high capacity retention of 95% even after 95 000 cycles.[163] Recently, Liu's group also found the ether-based electrolyte of 1 M $NaPF_6$ in diglyme can enhance the electrochemical performance of $Na_3(VOPO_4)_2F$ cathode (including cycling stability and initial Coulombic efficiency) due to the formation of robust and thin (serval nanometers) CEI layer, as shown in Figure 11b,c.[164] More importantly, they also proved that the decomposition of ether-based electrolytes is not always conducive to generating suitable CEI layers, since the combination of sodium salt and solvent can significantly affect the stability of organic–inorganic interphase. Based on the DFT

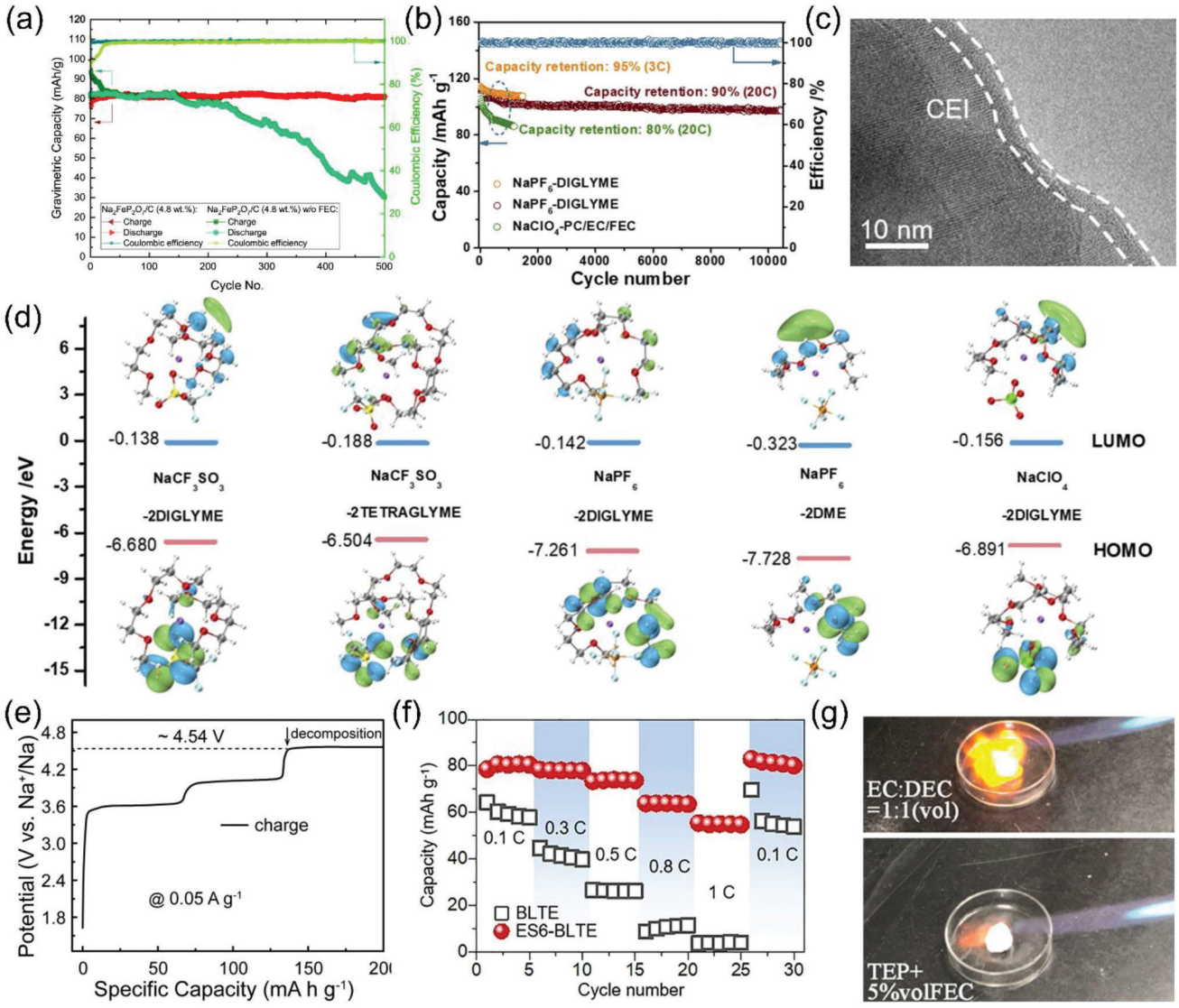

Figure 11. a) Cycling performance of $Na_2FeP_2O_7$/C at 1C in electrolytes with and without 5 wt% FEC. Reproduced with permission.[162] Copyright 2021, Elsevier. b) Cycling performance of $Na_3V_2O_2(PO_4)_2F$ cathode in different electrolytes. c) TEM image of the $Na_3V_2O_2(PO_4)_2F$ cathode after cycled in $NaPF_6$-diglyme electrolyte. d) DFT calculated HOMO and LUMO energy levels of salt-solvent complexes in various electrolytes. Reproduced with permission.[164] Copyright 2022, Elsevier. e) Initial charge curve of $Na_3V_2(PO_4)_2F_3$ cathode in the electrolyte of 3.04 m $NaPF_6$ in diglyme/DOL (10:1, by volume). Reproduced with permission.[166] Copyright 2021, Wiley-VCH. f) Rate performance of Na//$Na_3V_2(PO_4)_3$ cells at −40 °C in the electrolyte with and without ES additive. Reproduced with permission.[169] Copyright 2023, Wiley-VCH. g) Ignition test of the TEP electrolyte and the carbonate electrolyte. Reproduced with permission.[171] Copyright 2019, American Chemical Society.

calculation of HOMO and LUMO levels, the $NaPF_6$-diglyme system has a lower HOMO energy than $NaCF_3SO_3$-diglyme and $NaClO_4$-diglyme (Figure 11d), suggesting the better antioxidation ability of $NaPF_6$-diglyme electrolyte. Therefore, the synergy effect between ether solvent and sodium salt is necessary to stabilize the potential window and form the robust CEI layer. However, the common ether-based electrolytes still suffer from poor oxidation resistance and are susceptible to decomposition on the cathode surface under high redox potential, limiting their practical application.[165] Therefore, Wu et al. designed a novel electrolyte of 3.04 m $NaPF_6$ in diglyme with the addition of 1,3-dioxolane (DOL) diluent (10:1, by volume), and this electrolyte possesses high oxidative stability and can withstand a high voltage of 4.5 V (Figure 11e).[166] Compared with the electrolyte of 0.94 m $NaPF_6$ in diglyme, the high-voltage cathode of $Na_3V_2O_2(PO_4)_2F$ deliver a large reversible capacity of 107 mAh g^{-1} at 0.2 A g^{-1} even after 1600 cycles in the electrolyte of 3.04 m $NaPF_6$ in diglyme/DOL (10:1, by volume).

To enhance the practicality of phosphate-based polyanionic cathodes, it is not only necessary to perform well at ordinary temperatures, but also needs to adapt to extreme environments, such as high and low temperatures. Wang's group demonstrated that $Na_4Fe_3(PO_4)_2P_2O_7$ works well at ultralow temperature (−70 °C) and ultrahigh temperature (≥100 °C) in the ether-based

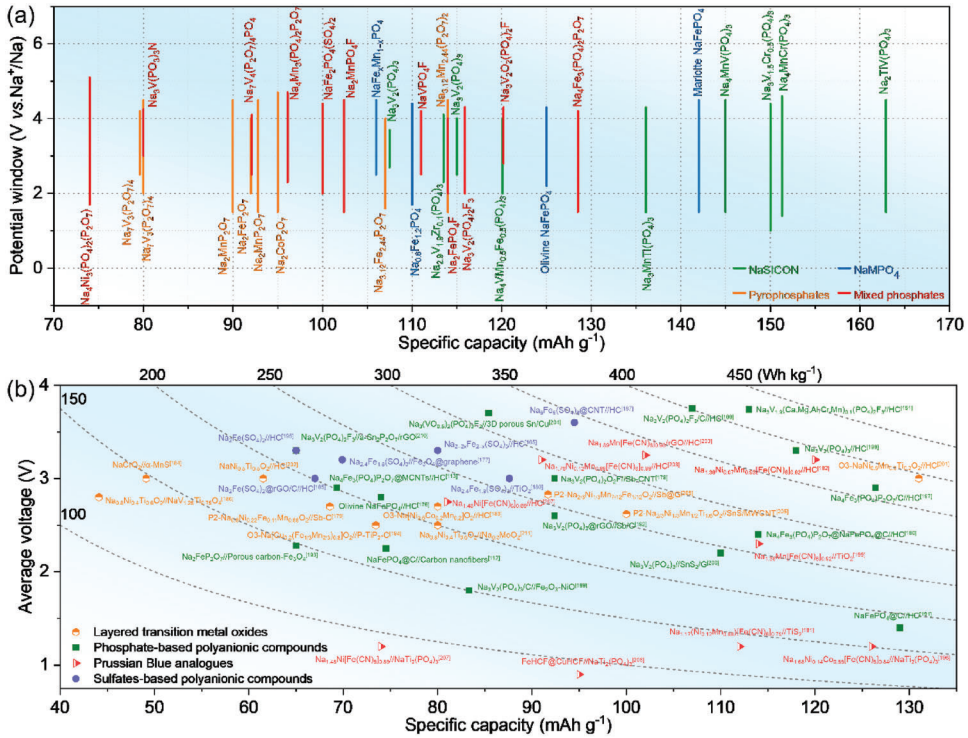

Figure 12. a) Comparison of specific capacities and average discharge redox voltages of various reported cathode materials. b) Average voltage, specific capacity, and the corresponding gravimetric energy density of promising commercial phosphate-based SIFCs (the specific capacities calculated based on the cathode).[112,113,151,176–211]

electrolyte of 1 M $NaPF_6$ in diglyme.[167,168] Very recently, Yu et al. designed a now low-temperature carbonate electrolyte of 1 M NaFSI in EC/PC/DEC (1:1:1, v/v) with 6% ethylene sulfate (ES), and the initial capacity of $Na_3V_2(PO_4)_3$//Na is as high as 84 mAh g^{-1} with a capacity retention of ≈65.5% at 1 C under −40 °C (Figure 11f).[169] This is because ES additive can effectively accelerate the desolvation kinetics of Na^+ by weakening the Na^+-solvent interaction, and the corresponding SEI layer is rich in Na_3N, Na_2S, and Na_2SO_4 with excellent ionic conductivity and mechanical strength (≈7.0 GPa). To achieve a stable operation at the high-temperature condition (>60 °C), some flame-retardant electrolytes were reported for improving the thermal stability of SIBs. For example, Balaya et al. and Cao et al. designed 1 M $NaBF_4$/tetraglyme and 0.9 M $NaClO_4$/triethyl phosphate as the flame-retardant electrolytes (Figure 11g), respectively, simultaneously realizing the outstanding sodium-storage performance of $Na_3V_2(PO_4)_3$ cathode.[170,171] Meanwhile, ionic liquids have also been used to realize the nonflammability of phosphate-based polyanionic cathodes or enhance the related sodium-storage capability, such as fast electrochemical kinetics, large reversible capacity, and long cycle life.[172–174]

5. From Material to Practical Application

5.1. Electrochemical Performance Analysis in Different Battery Prototypes

We have described overall the family of phosphate-based polyanionic cathodes for SIBs, and the general modification strategies on the material level are also summarized to enhance the sodium-storage performance of phosphate-based polyanionic cathodes. Simultaneously, **Figure 12**a presents data on the specific capacity versus potential window for phosphate-based polyanionic compounds in SIBs systems. In the half-cell configuration, the energy density of phosphate-based polyanionic cathodes is as high as 566 Wh kg^{-1} (vs Na foil), which has exceeded that of $LiFePO_4$.[175] However, the electrochemical performance of the cathode materials in the half cell is of limited reference significance for the design and development of practical battery, since the research of SIBs should be application-oriented scientific engineering. Hence, it is more holistic in reflecting the application potential of the cathodes based on the relevant sodium-ion full cells (SIFCs) data. Depending on the difference in the manufacturing process, such as the internal device structure and packaging form, the general prototypes of SIFCs include coin cell, pouch cell, and cylindrical cell. Among them, coin cell is the most common in the research articles and can explore the practical performance of phosphate-based polyanionic cathodes to a certain. Meanwhile, a comparison of energy density and specific capacity between the phosphate-based polyanionic cathodes and other cathodes in SIFCs is shown in Figure 12b, where the phosphate-based full cells display relatively high operating voltages and high energy densities.

In comparison with the conventional metal shells of batteries, pouch cells offer the advantages of high safety, light weight, low internal resistance, and design flexibility. The frequency of the pouch cell appearing in the research articles has gradually increased with the update of battery manufacturing equipment

in the laboratory. For example, Wu and co-workers designed the HC//$Na_3V_2(PO_4)_2F_3$ pouch cell, which can light up 63 red LED bulbs.[212] Similarly, Yang et al. used $Na_3V_2(PO_4)_3$ and HC as the cathode and anode, respectively, and the assembled pouch cell possesses a capacity of 385 mAh and capacity retention of 85.1% after 120 cycles).[213] Recently, Cao's group assembled 3500 mAh pouch cell using $Na_4Fe_{2.91}P_4O_{14.91}$ cathode and HC anode, and a high discharge capacities of 3133 mAh and 2814 mAh are maintained even at a high current density of 5 C and low operation temperature of −40 °C, respectively.[214] These results demonstrate that phosphate-based polyanionic cathodes have promising potential to achieve the practical application of SIBs. Besides, cylindrical cells as the relatively mature type have a high degree of automation, stable product quality, and low cost. The typical models of cylindrical cells include 14 650, 18 650, 21 700, 26 650, 32 650, etc., named based on their size, and 18 650/26 650-size cylindrical cells have been widely used in the current battery market. In general, the 26650-size cylindrical cell has a larger capacity and lower cost than 18650-size cylindrical cell. Hu et al. reported $Na_3(VOPO_4)_2F$-26650 cylindrical cell with the HC as the anode, which has a larger energy density of ≈100 Wh kg^{-1} and a high capacity retention of 95.2% even after 2000 cycles.[114]

It is worth noting that all these prototypes of SIFCs follow the same design principles: 1) the matching between cathode and anode is essential for stimulating the electrochemical performance of the SIFCs and avoiding the waste of electrode materials; 2) the reasonable compaction density can not only reduce the electrode volume to boost the energy density of SIFCs, but also increase the contact between the active particles and the conductive carbon to improve electrochemical performance. Nevertheless, the lack of uniform specifications for parameters (such as mass loading, electrode thickness, and size) reported in research articles resulted in the limited guidance for the commercial application of the materials in question, and direct comparison with traditional commercial data is not possible. Therefore, the full-cell configuration for phosphate-based cathodes should be designed based on the needs of the application terminal as much as possible for increasing the practicality of the test data.

5.2. Analysis of Industrialization and Cost

The commercial development of SIBs is in full swing, and the SIBs' market is mainly composed of three parts: electrode material suppliers (i.e., Wenzhou Nashu, Shenzhen Janaenergy, and Zhejiang Natrium), start-up SIBs companies (i.e., HiNa, Tiamat, Altris, Faradion, and Natron Energy), and mature LIBs companies (i.e., CATL, ATL, Guangzhou Great power, and EVE). Among them, the main products of Shenzhen Janaenergy is Fe-based phosphates (i.e., $Na_4Fe_3(PO_4)_2P_2O_7$), whereas the specific sodium-storage performance of these commercial phosphate-based polyanionic cathodes is still unclear. Besides, Tiamat as a start-up company was established in 2017, came out of the French network for electrochemical energy storage supported by the French National Centre for Scientific Research. This company adopts the technology route of $Na_3V_2(PO_4)_2F_3$ cathode and HC anode, and the as-assembled SIBs have a high energy density (100–120 Wh kg^{-1}), long cycle life (capacity retention of 80% after 5000 cycles) and superior power density (>5000 W kg^{-1}). Meanwhile, their SIBs are mainly used in static energy storage and power vehicles (48 V mild hybrid vehicles, 12 V starting lighting and ignition, fast charging electric buses, etc.), and it is expected that the production capacity will reach 6 GWh by 2030. However, there is no large-scale production. Apart from the start-up battery companies, some mature LIBs companies have also begun to lay out in the field of phosphate-based cathodes for SIBs. Very recently, Guangzhou Great Power claimed two types of electric cores for SIBs, which have large energy density (145 Wh kg^{-1}), stable cycling performance (>3000 cycles), wide working temperature (−40–55 °C), and excellent capacity retention (>96% at 60 °C for 7 days).

As described above, these companies choose different phosphate-based polyanionic compounds as the technical reserves, which might be because their strategic goals are not aligned. For example, the NASICON-structure cathode materials generally have high ionic conductivity and robust crystalline structure, demonstrating potential to approach $LiFePO_4$, and have been produced in small batches. However, the high price and toxicity of V inevitably limited its large-scale application for SIBs. Therefore, Fe-based phosphates with low cost and wide source of raw materials become the future development direction of phosphate-based polyanionic cathodes for SIBs. Among various Fe-based phosphates, $Na_4Fe_3(PO_4)_2P_2O_7$ is a promising candidate cathode material for SIBs because of its high electrochemical performance, environmental friendliness, and low cost. Notably, some electrochemically inactive impurities (i.e., maricite $NaFePO_4$) can occur during the preparation process, further affecting the electrochemical performance. Therefore, it is urgent to explore a facile and scalable method with low cost to realize large-scale production of high-performance $Na_4Fe_3(PO_4)_2P_2O_7$ without inactive impurities for practical applications.

Fundamentally, the difficulties in industrializing phosphate-based polyanionic cathodes for SIBs lie in cost reduction and process optimization. For cost reduction, the accepted methods include 1) exploring low-cost scale-up preparation methods and 2) developing V-free phosphate cathode materials. In general, the conventional preparation processes of phosphate-based polyanionic compounds can be mainly categorized into solid-state methods (i.e., high-temperature solid-state method, mechanical ball milling method, and microwave heating method) and liquid-state methods (i.e., hydrothermal/solvothermal method, sol-gel method, and spray drying method). Although the solid-state methods have a relatively simple process and low preparation cost, easily realizing large-scale production, the mixing uniformity of the product is relatively poor, resulting in unsatisfactory electrochemical properties. In contrast, the liquid-state methods have the advantage of high product quality, but the high difficulty of process control and complexity of the process make it difficult to achieve cost controllability. However, according to the latest literature, the mechanochemical method without solvent and high-temperature treatment is a new synthesis method to achieve the large-scale production of low-cost phosphate-based polyanionic cathode materials.

Phosphate-based polyanionic cathode materials generally show poor intrinsic conductivity and undesirable kinetic performance, thus it is necessary to modify their electrochemical

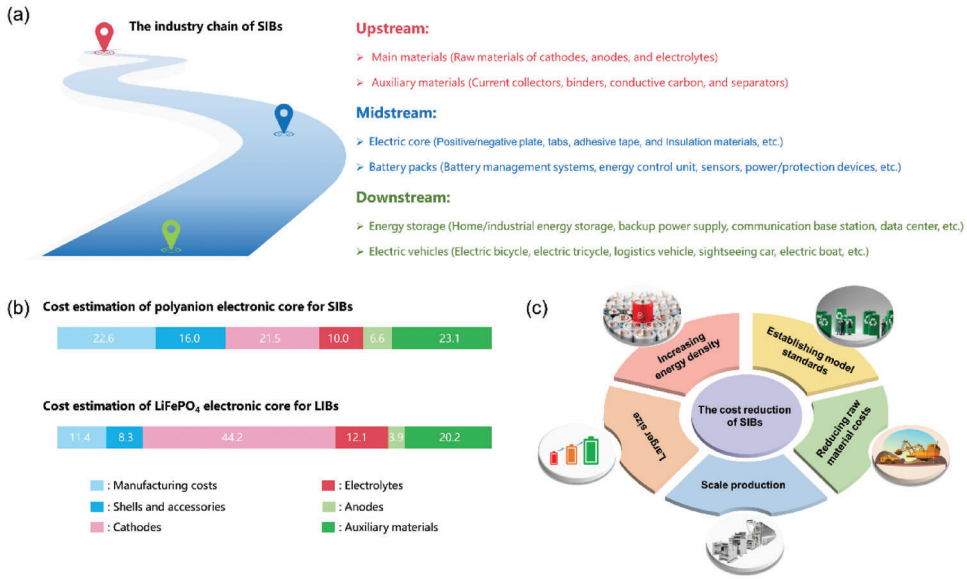

Figure 13. a) The industry chain structure of SIBs. b) Cost estimations of polyanion electric core for SIBs and $LiFePO_4$ electric core for LIBs. c) The corresponding strategies for reducing the cost of SIBs.

performance by suitable process optimization strategies. However, the relevant modification technology often relies on long-term process accumulation and significant R&D investment, leading to high technical barriers. In conjunction with the industrialization progress of phosphate-based polyanionic cathodes for SIBs, the unsatisfactory electrochemical performance is indeed one of the main factors restricting their further development. Therefore, the updated iteration of sodium-storage capability for phosphate-based polyanionic cathodes remains a top priority. Based on the patent portfolios of major battery manufacturers in the field of phosphate-based cathode materials, the mainstream modification strategies at the industrial level include surface coating, ion doping, and nanosizing, or the efficient combination of these strategies. However, their intrinsic shortcomings still limit their application potential in industrialized production. For example, a moderate amount of conductive material coating boosts the crystalline structural stability and surface electronic conductivity of phosphate-based polyanionic cathodes to a certain extent. Nevertheless, the excessive induction of coating materials can lengthen the Na^+ pathways and reduce the specific capacity, thus weakening the electrochemical performance of the practical SIBs. Similarly, too much ion doping can also affect the electrochemical performance of phosphate-based polyanionic cathodes due to the generation of impurities with negative effects. In addition, during the industrial production process, the nanosizing treatment of phosphate-based cathodes generally causes excessive energy consumption, and the relatively complex process means higher production costs. These are contrary to the concept of the low cost of SIBs. Hence, in the industrial production process, the reasonable design of modification strategies is crucial for the large-scale production of phosphate-based polyanionic cathodes. The next generation of ideal optimization methods at the industrialization level may be based on efficient interfacial modification and intrinsic crystal structure optimization, namely the improvement in surface electronic conductivity, ionic conductivity, and structure reversibility.

The technological maturity of SIBs is not as high as that of LIBs, and SIBs are still in the transitional stage from the introduction phase to the growth phase. Although SIBs have not yet formed an industrial scale and possess high technological barriers, their cost advantages become increasingly evident in the context of high-cost Li_2CO_3. Meanwhile, the development space of SIBs has further expanded benefiting from the increasing demand for large-scale energy storage systems. The industry chain of SIBs is shown in **Figure 13**a, and the midstream (electric core and battery packs) and downstream (application scenarios) of the industry chain are mainly determined by the product characteristics of upstream, namely the cost and electrochemical performance of electrodes and the compatibility of various auxiliary materials. Furthermore, in terms of the cost of polyanionic electric cores for SIBs, the cost ratio of the cathode is 21.51%, accounting for the highest proportion, but it is still far lower than the proportion of the cathode in the cost of $LiFePO_4$ electric core (≈41.17%), as shown in Figure 13b. Nevertheless, the cost of manufacturing, shells, and accessories for SIBs is almost twice that for LIBs (38.6% vs 19.7%), which is because the volume capacity density of SIBs' polyanionic electric core is lower than that of $LiFePO_4$ electric core, consuming more consumables and packaging. Based on the above discussion, the overall cost of SIBs is determined by multiple factors, such as the electrochemical performance of electrodes, the cost of raw materials, and the cost of packaging. In theory, SIBs have significant cost advantages, but currently, there is still a gap in the electrochemical performance of conventional phosphate-based cathodes for SIBs compared to $LiFePO_4$ for LIBs, hindering the commercial progress of phosphate-based cathodes. Meanwhile, if the technological progress and market scale of phosphate-based cathodes are not ideal, it will cause a lower overall cost-reduction rate than

expected for SIBs, further delaying the commercialization degree of phosphate-based cathodes. Besides, the formation of the industrial chain of phosphate-based cathodes for SIBs requires cooperation between upstream and downstream enterprises rather than purely technical factors. More importantly, the significant external factor driving the rapid development of SIBs is the high price of Li salts. When the cost of Li salts falls back to a relatively low level in the future, and the industry chain of SIBs is not yet perfect, so the industry of phosphate-based cathodes may face the problem of insufficient development potential. Furthermore, in addition to phosphate-based polyanionic compounds, all sulfate-based polyanionic compounds, layered transition metal oxide, and PBAs as the cathode for SIBs have exhibited promising commercial potential. Their rapid development will squeeze the development space of phosphate-based cathodes, so making the development of high-performance phosphates even more urgent.

Therefore, it still requires more effective strategies to further reduce the cost of SIBs, as shown in Figure 13c. In detail, 1) increasing the energy density of polyanionic electric cores through advanced battery structure design and electrochemical performance optimization; 2) producing larger-sized SIBs to reduce the impact of auxiliary materials (i.e., shell, separator, and binders) on the total energy density; 3) reducing the cost of raw materials, such as electrode raw materials, electrolyte raw materials, and raw materials for auxiliary materials; 4) achieving the scale production of SIBs for reducing the cost and depreciation loss of battery production equipment; 5) developing a unified battery model to guide product design and manufacturing processes, and ensuring product yield and consistency of SIBs.

In summary, SIBs have a wide range of application prospects in scenarios that do not require high energy density, such as large electric vehicles, low-speed four-wheelers, household energy storage products, and large-scale smart grids, and will have a place after large-scale commercialization. Therefore, considering the trade-off between cost and performance, some low-cost phosphate-based polyanionic cathodes, such as Fe/Mn-based phosphates, are expected to be applied in the large-scale energy storage system with ultra-long cycle life.[215]

6. Conclusion and Perspective

6.1. Conclusion

Phosphate-based polyanionic compounds, as one of the most promising cathodes for SIBs, possess abundant species, superb structural/thermal stability, and high operation voltages, mainly including phosphates, pyrophosphates, and mixed phosphates. In this review, the crystal structures, sodium-storage mechanisms, and recent progress of several typical phosphate-based polyanionic compounds have been systematically discussed. Meanwhile, we also summarized the powerful modification methods in response to the thorny sodium-storage problems of phosphate-based cathodes. Besides, we described the recent progress of phosphate-based cathodes in laboratory-scale SIFCs and evaluated the application potential based on the electric core structure cost and worldwide commercialization degree of phosphate-based polyanionic compounds.

According to literature reports, the electrochemical performance of many phosphate-based polyanionic compounds begins approaching that of $LiFePO_4$ cathode for LIBs. Among them, V-based phosphates, such as $Na_3V_2(PO_4)_3$ and $Na_3(VO_{1-x}PO_4)_2F_{1+2x}$, show great commercialization potential, benefiting from their high operation voltages, superior cycling performance, and large reversible capacities. However, the relatively high cost and toxicity of V and F increase production costs. Hence, some low-cost phosphates have also been researched and exhibited excellent sodium-storage performance, such as $Na_4Fe_3(PO_4)_2P_2O_7$, $NaFePO_4$, and $Na_2FeP_2O_7$. Due to the relatively low redox potentials of Fe-based phosphates, their energy densities are not large enough to adapt to different applications. Nevertheless, considering the cost advantage, Fe-based phosphates may be superior to V-based phosphates in large-scale energy storage with low requirements for energy density. All these phosphate-based polyanionic compounds have shown great potential in practical applications, whereas the challenges associated with developing them remain enormous. For instance, phosphate-based polyanionic cathodes are trapped in the intrinsic low electronic conductivity, causing the sluggish electrochemical kinetics. Besides, the relatively high operation voltage of phosphate-based polyanionic compounds might put the electrolytes at risk of decomposition, further limiting the energy density of some phosphates with high redox potential (i.e., $Na_4Ni_3(PO_4)_2P_2O_7$ and $Na_4Co_3(PO_4)_2P_2O_7$). Moreover, to address the issue of limited specific capacity, the anion-substituted or off-stoichiometric phosphate-based polyanionic compounds, such as $Na_3(VO_{1-x}PO_4)_2F_{1+2x}$ and $Na_{3.32}Fe_{2.34}(P_2O_7)_2$, were reported through reducing the overall molecular weight or activating more electrons during (de)sodiation process. At the same time, the phosphate-based polyanionic compounds, such as $Na_4FeV(PO_4)_3$, $Na_4MnV(PO_4)_3$, and $Na_2MnTi(PO_4)_3$, exhibit relatively large reversible capacities due to the wide potential window, but the high depths of charge/discharge may cause the crystalline structure instability. Until now, numerous phosphate-based polyanionic compounds have been reported and possess large reversible capacities, high average voltages, long cycle lives, or low cost, so phosphate-based polyanionic cathodes can meet suitable for different application scenarios, such as low-speed electric vehicles and large-scale smart grids.

While many phosphate-based polyanionic compounds have shown promising application potential, their intrinsic defects (i.e., poor conductivity and limited energy density) still hinder practical performance. Therefore, many material-level strategies have been performed to narrow the gap between the theoretical and practical performance of phosphate-based polyanionic compounds. In the final analysis, these strategies are all aimed at improving the specific capacity, cycle life, rate performance, and average voltage of phosphate-based polyanionic cathodes (**Figure 14**). 1) For boosting the specific capacity, the effective strategy is to increase the number of electrons involved in the (de)sodiation process, and the specific methods include ion doping/substitution, nanomorphology design, electrolyte optimization, off-stoichiometric phase engineering, operation conditions regulation, and anion substitution. 2) For improving the rate performance, the strategies of carbon coating, ion doping, morphology design, and electrolyte optimization have been performed according to the improvement of electronic/ionic transfer. 3) For increasing average voltage, the core idea is to increase the redox potential through the solutions of regulating redox couples,

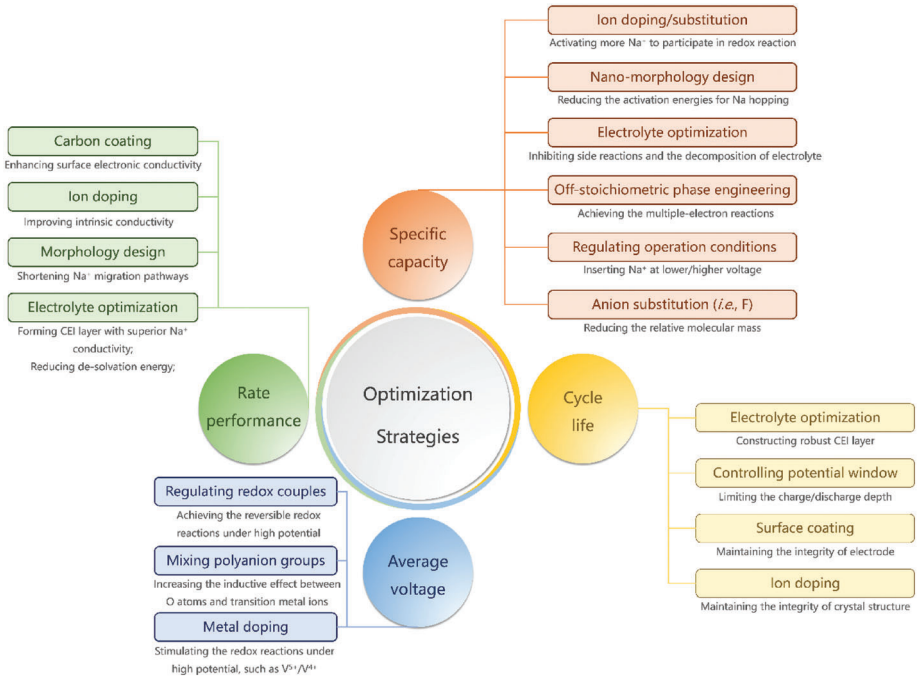

Figure 14. The mainstream strategies to improve specific capacity, rate performance, average voltage, and cycle life of phosphate-based polyanionic compounds from material level.

mixing polyanion groups, and ion doping. 4) For modifying the cycle life, electrolyte optimization, controlling potential window, surface coating, and ion doping are conducted to construct stable electrode/crystal structures or form robust CEI layers. Noticeably, although surface coating and morphological control can boost the electrochemical performance of phosphate-based polyanionic compounds, these strategies eventually affect the performance of practical SIBs. This is because they can decrease the practical capacity or compacted density of the electrode, impairing the energy/volume density of the resulting SIBs. Furthermore, the production costs of SIBs can also be increased due to the need for more accessory materials, such as larger battery shells, more current collectors, and more separators. Hence, some emerging modification strategies (i.e., ion doping and electrolyte optimization) have been widely researched for their ability to improve the rate performance without the effect on the compacted density. However, the specific working mechanisms are relatively complex, and further exploration is needed. The relatively high cost of some special electrolytes (i.e., high-concentration electrolytes, ether-based electrolytes, and ionic liquids) is also a knotty problem. It is worth noting that all the above-mentioned strategies are based on the laboratory scale far from practically relevant ones, so the corresponding results may not be able to completely reflect their promise in practical batteries. Considering that the research on optimizing the electrochemical performance of phosphate-based polyanionic compounds aims to improve the practical SIBs' performance, we believe the rational composite design strategy of thin carbon coating and high-entropy metal doping/substitution can achieve the practical application of phosphate-based polyanionic cathodes in SIBs.

At the material level, phosphate-based polyanionic compounds have shown excellent sodium-storage performance in both half-cell and full-cell configurations. Moreover, according to the relevant electrochemical performance in different SIBs' prototypes, phosphate-based polyanionic cathodes has the potential for commercial development. However, these SIFCs are mostly still on a laboratory scale and lack unified specifications, so the results cannot be directly compared with the traditional commercial LIBs' data and guide the commercial application of phosphate-based polyanionic cathodes in practical SIBs. From a cost perspective, the cost advantage of SIBs is greatly based on the ultrahigh price of Li_2CO_3. Currently, with the price reduction of Li_2CO_3, it is needed to re-estimate the advantages of SIBs in comparison with that of LIBs and identify the niche of SIBs for driving their rapid development. Just like the first-generation LIBs, the success is closely related to the rise of portable electronic devices. In addition, because of the relatively small energy density, the packaging cost of SIBs with polyanionic cathodes is higher than that of $LiFePO_4$ batteries. Thus, it is necessary to develop a comprehensive strategy for reducing the total cost of SIBs, which can refer to Figure 13c. At present, the industrialization process of SIBs has achieved a smooth transition from the emerging stage to the growth stage, but there is still a significant gap from the maturity stage. Noticeably, the continuous increase in the number of startup SIBs' companies is a positive sign, which can also ensure the success and commercialization of SIB technology in the coming years.

6.2. Perspective

Considering the intrinsic characteristics of phosphate-based polyanionic compounds, the improvement of the practicality still needs to be based on the material level. Therefore, we

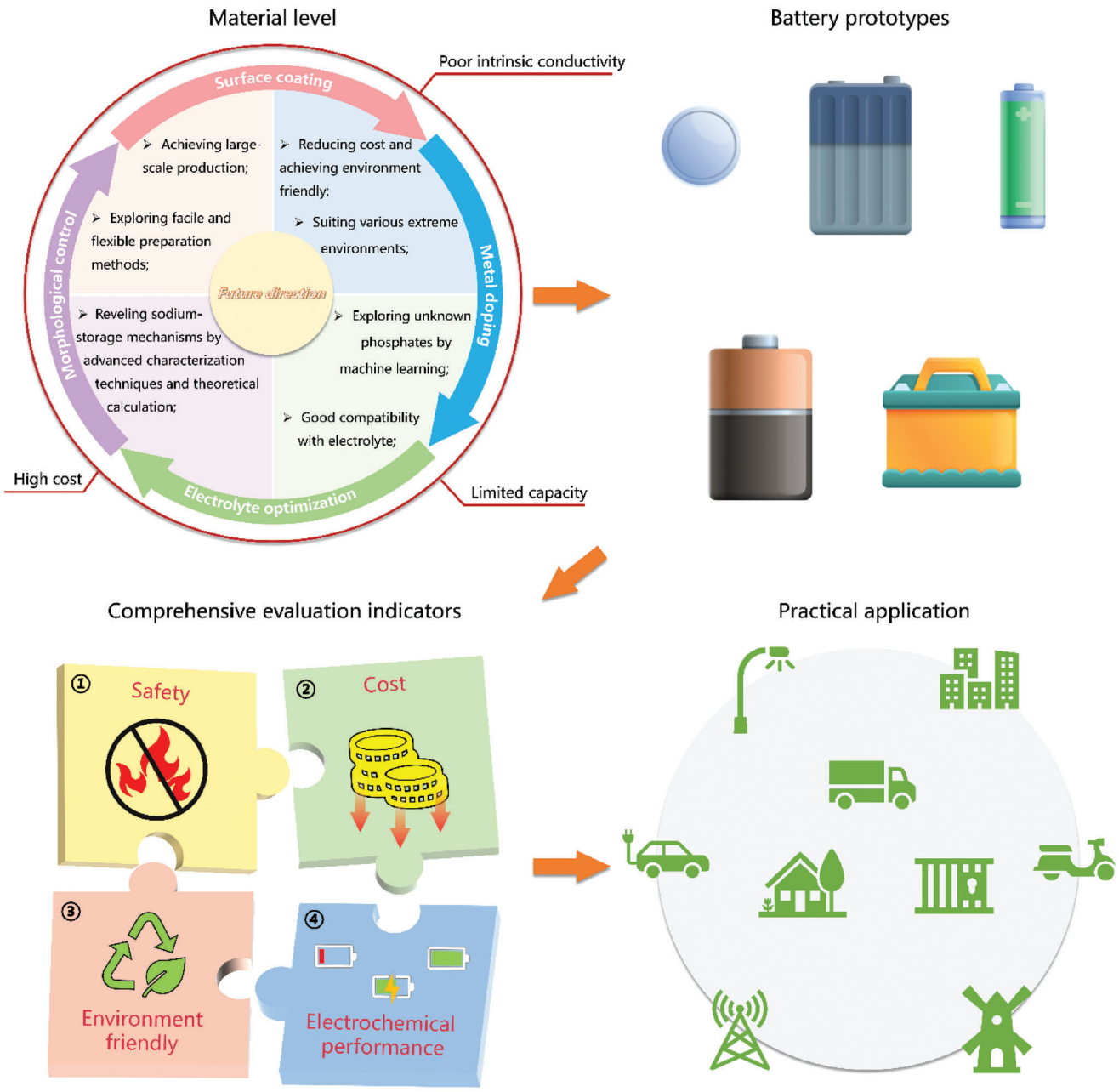

Figure 15. The future direction of phosphate-based polyanionic cathodes for SIBs toward commercialization.

suggest that the future research on phosphate-based polyanionic cathode materials for SIBs should concentrate on the following directions, as shown in **Figure 15**: 1) It is meaningful for the commercialization to achieve the large-scale production of polyanionic cathode materials with excellent sodium-storage performance through facile and flexible methods; 2) To reduce cost and achieve environmental friendliness, exploring the low-cost Fe/Mn-based phosphates with high performance is an effective method to avoid the excessive utilization of V element; 3) The obscure mechanisms (including the promotion of ion doping and the formation of CEI layers) need to be further explored by using advanced characterization techniques and theoretical calculation; 4) To achieve the practical application of phosphate-based cathodes in large-scale storage field, it is critical to possess high safety and remarkable sodium-storage performance in the wide temperature for suiting various extreme conditions; 5) Due to the limited cathode materials reported so far, the use of powerful machine learning method will gradually become popular to explore unknown phosphates with excellent sodium-storage properties.

Besides, various preparation methods (i.e., solid-state reactions, hydro/solvothermal reactions, coprecipitation, and spray pyrolysis) have been applied to synthesize phosphate-based

polyanionic cathode materials for SIBs. Among these mainstream synthetic processes, mechanical ball milling, coprecipitation, and sol-gel methods have shown excellent practical application potential due to the low energy consumption, high product purity, low equipment requirements, and/or low industrialization difficulty. Meanwhile, the development of suitable preparation methods can also greatly decrease the production cost of phosphate-based polyanionic cathode materials for SIBs. Given that the electrochemical performance of practical SIBs is also related to the pack process, the optimization of the electric core structure with phosphate-based polyanionic cathodes from LIBs is greatly possible to increase the performance of SIBs, not limited to large cylindrical batteries and large pouch cells. For instance, the electric core structure with phosphate-based polyanionic cathodes may draw on the experience of the blade battery for improving energy density and safety. Besides, it is crucial to unify the comprehensive evaluation criteria of phosphate-based polyanionic compounds in different SIBs' prototypes, which should contain safe, cost, environment-friendly, and electrochemical performance. Currently, research on the safety of SIBs is mostly based on the laboratory level, so SIBs may face similar safety issues as LIBs after entering practical applications. The negative impact of safety accidents will seriously damage the competitiveness and industrial progress of SIBs. This requires improving SIBs' safety performance from battery structure design and electrode/electrolyte optimization. Hence, it is meaningful for phosphate-based polyanionic compounds to improve their compatibility with battery structures and fire-retardant electrolytes. Meanwhile, to reduce the cost and achieve environment friendly practical SIBs, the best choice for phosphate-based polyanionic cathodes is to adopt Fe/Mn-based phosphates, avoiding the high-cost or toxic elements, such as V, Cr, Ni, Co, and F. In summary, we hope that phosphate-based polyanionic compounds can promote the industrial development of SIBs and meet the different needs of human society.

Acknowledgements

This work was supported by the National Natural Science Foundation of China (52202286, 52250710680, 51971124, 52171217), Zhejiang Provincial Natural Science Foundation of China (LZ21E010001), Science and Technology Project of State Grid Corporation of China (5419-202158503A-0-5-ZN), WenZhou Natural Science Foundation (G20220016, ZG2022032).

Conflict of Interest

The authors declare no conflict of interest.

Keywords

commercialization process, electrochemical performances, optimization strategies, phosphate-based polyanionic compounds, sodium-ion batteries

Received: May 30, 2023
Revised: July 25, 2023
Published online:

[1] V. Etacheri, R. Marom, R. Elazari, G. Salitra, D. Aurbach, *Energy Environ. Sci.* **2011**, *4*, 3243.
[2] H. Pan, Y.-S. Hu, L. Chen, *Energy Environ. Sci.* **2013**, *6*, 2338.
[3] H. Li, M. Xu, H. Long, J. Zheng, L. Zhang, S. Li, C. Guan, Y. Lai, Z. Zhang, *Adv. Sci.* **2022**, *9*, 2202082.
[4] Y. Li, Y. S. Hu, M. M. Titirici, L. Chen, X. Huang, *Adv. Energy Mater.* **2016**, *6*, 1600659.
[5] L. F. Zhao, Z. Hu, W. H. Lai, Y. Tao, J. Peng, Z. C. Miao, Y. X. Wang, S. L. Chou, H. K. Liu, S. X. Dou, *Adv. Energy Mater.* **2021**, *11*, 2002704.
[6] Y. Katsuyama, Y. Nakayasu, H. Kobayashi, Y. Goto, I. Honma, M. Watanabe, *ChemSusChem* **2020**, *13*, 5762.
[7] M. Chen, Q. Liu, S. W. Wang, E. Wang, X. Guo, S. L. Chou, *Adv. Energy Mater.* **2019**, *9*, 1803609.
[8] L. Gan, X.-G. Yuan, J.-J. Han, J. Li, L. Zheng, H.-R. Yao, *Carbon Neutralization* **2023**, *2*, 235.
[9] X. Cao, A. Pan, S. Liu, J. Zhou, S. Li, G. Cao, J. Liu, S. Liang, *Adv. Energy Mater.* **2017**, *7*, 1700797.
[10] L. Xu, H. Li, T. Du, Q. Xue, Y. Gao, Z. Yu, H. Bai, *Battery Energy* **2023**, *2*, 20220054.
[11] J. Li, H. Hu, J. Wang, Y. Xiao, *Carbon Neutralization* **2022**, *1*, 96.
[12] A. Yamada, *Molecules* **2021**, *26*, 5143.
[13] Y. Liu, J. Li, Q. Shen, J. Zhang, P. He, X. Qu, Y. Liu, *eScience* **2022**, *2*, 10.
[14] Y. Huang, Y. Zheng, X. Li, F. Adams, W. Luo, Y. Huang, L. Hu, *ACS Energy Lett.* **2018**, *3*, 1604.
[15] M. Chen, Q. Liu, Y. Zhang, G. Xing, S.-L. Chou, Y. Tang, *J. Mater. Chem. A* **2020**, *8*, 16061.
[16] C. Masquelier, L. Croguennec, *Chem. Rev.* **2013**, *113*, 6552.
[17] Y. Gao, H. Zhang, X. H. Liu, Z. Yang, X. X. He, L. Li, Y. Qiao, S. L. Chou, *Adv. Energy Mater.* **2021**, *11*, 2101751.
[18] X. Pu, H. Wang, T. Yuan, S. Cao, S. Liu, L. Xu, H. Yang, X. Ai, Z. Chen, Y. Cao, *Energy Storage Mater.* **2019**, *22*, 330.
[19] Q. Li, B. Lin, S. Zhang, C. Deng, *J. Mater. Chem. A* **2016**, *4*, 5719.
[20] R. Xu, N. Sun, H. Zhou, X. Chang, R. A. Soomro, B. Xu, *Battery Energy* **2023**, *2*, 20220054.
[21] J. He, T. Tao, F. Yang, Z. Sun, *ChemSusChem* **2022**, *15*, 202200817.
[22] Y. Niu, Y. Zhao, M. Xu, *Carbon Neutralization* **2023**, *2*, 150.
[23] J. Gopalakrishnan, K. K. Rangan, *Chem. Mater.* **1992**, *4*, 745.
[24] J. Barker, M. Saidi, J. Swoyer, *Electrochem. Electrochem. Solid State* **2002**, *6*, A1.
[25] F. Sauvage, E. Quarez, J.-M. Tarascon, E. Baudrin, *Solid State Sci.* **2006**, *8*, 1215.
[26] R. Gover, A. Bryan, P. Burns, J. Barker, *Solid State Ionics* **2006**, *177*, 1495.
[27] P. Moreau, D. Guyomard, J. Gaubicher, F. Boucher, *Chem. Mater.* **2010**, *22*, 4126.
[28] B. Ellis, W. Makahnouk, Y. Makimura, K. Toghill, L. Nazar, *Nat. Mater.* **2007**, *6*, 749.
[29] J. Kim, D.-H. Seo, H. Kim, I. Park, J.-K. Yoo, S.-K. Jung, Y.-U. Park, W. A. Goddard III, K. Kang, *Energy Environ. Sci.* **2015**, *8*, 540.
[30] T. Honma, T. Togashi, N. Ito, T. Komatsu, *J. Ceram. Soc. Jpn.* **2012**, *120*, 344.
[31] H. Kim, I. Park, S. Lee, H. Kim, K.-Y. Park, Y.-U. Park, H. Kim, J. Kim, H.-D. Lim, W.-S. Yoon, K. Kang, *Chem. Mater.* **2013**, *25*, 3614.
[32] P. Barpanda, T. Ye, M. Avdeev, S.-C. Chung, A. Yamada, *J. Mater. Chem. A* **2013**, *1*, 4194.
[33] M. Nose, H. Nakayama, K. Nobuhara, H. Yamaguchi, S. Nakanishi, H. Iba, *J. Power Sources* **2013**, *234*, 175.
[34] S. Y. Lim, H. Kim, J. Chung, J. H. Lee, B. G. Kim, J.-J. Choi, K. Y. Chung, W. Cho, S.-J. Kim, W. A. Goddard III, *Proc. Natl. Acad. Sci. USA* **2014**, *111*, 599.

[35] H. Kim, C. S. Park, J. W. Choi, Y. Jung, *Angew. Chem., Int. Ed.* **2016**, *55*, 6662.
[36] W. Zhou, L. Xue, X. Lü, H. Gao, Y. Li, S. Xin, G. Fu, Z. Cui, Y. Zhu, J. B. Goodenough, *Nano Lett.* **2016**, *16*, 7836.
[37] C. W. Mason, F. Lange, *ECS Electrochem. Lett.* **2015**, *4*, A79.
[38] H. Gao, J. B. Goodenough, *Angew. Chem., Int. Ed.* **2016**, *55*, 12768.
[39] Y. Qi, Z. Tong, J. Zhao, L. Ma, T. Wu, H. Liu, C. Yang, J. Lu, Y.-S. Hu, *Joule* **2018**, *2*, 2348.
[40] Q. Zhang, X. Shen, Q. Zhou, K. Li, F. Ding, Y. Lu, J. Zhao, L. Chen, Y.-S. Hu, *Energy Mater. Adv.* **2022**, *2022*, 9828020.
[41] A. Zhao, T. Yuan, P. Li, C. Liu, H. Cong, X. Pu, Z. Chen, X. Ai, H. Yang, Y. Cao, *Nano Energy* **2022**, *91*, 106680.
[42] G. Ali, J.-H. Lee, D. Susanto, S.-W. Choi, B. W. Cho, K.-W. Nam, K. Y. Chung, *ACS Appl. Mater. Interfaces* **2016**, *8*, 15422.
[43] J. Zhang, X. Zhou, Y. Wang, J. Qian, F. Zhong, X. Feng, W. Chen, X. Ai, H. Yang, Y. Cao, *Small* **2019**, *15*, 1903723.
[44] P. Barpanda, G. Liu, C. D. Ling, M. Tamaru, M. Avdeev, S.-C. Chung, Y. Yamada, A. Yamada, *Chem. Mater.* **2013**, *25*, 3480.
[45] K. Shiva, P. Singh, W. Zhou, J. B. Goodenough, *Energy Environ. Sci.* **2016**, *9*, 3103.
[46] Y. Liu, Y. Zhou, J. Zhang, Y. Xia, T. Chen, S. Zhang, *ACS Sustainable Chem. Eng.* **2017**, *5*, 1306.
[47] W. Li, J. Li, R. Li, X. Li, J. Gao, S.-M. Hao, W. Zhou, *Battery Energy* **2022**, *1*, 20220006.
[48] K. Kawai, D. Asakura, S.-i. Nishimura, A. Yamada, *Chem. Mater.* **2021**, *33*, 1373.
[49] K. Kawai, W. Zhao, S.-i. Nishimura, A. Yamada, *ACS Appl. Energy Mater.* **2018**, *1*, 928.
[50] S. Chen, C. Wu, L. Shen, C. Zhu, Y. Huang, K. Xi, J. Maier, Y. Yu, *Adv. Mater.* **2017**, *29*, 1700431.
[51] Z. Jian, C. Yuan, W. Han, X. Lu, L. Gu, X. Xi, Y. S. Hu, H. Li, W. Chen, D. Chen, Y. Ikuhara, L. Chen, *Adv. Funct. Mater.* **2014**, *24*, 4265.
[52] Z. Jian, W. Han, X. Lu, H. Yang, Y. S. Hu, J. Zhou, Z. Zhou, J. Li, W. Chen, D. Chen, *Adv. Energy Mater.* **2013**, *3*, 156.
[53] M. Pivko, I. Arcon, M. Bele, R. Dominko, M. Gaberscek, *J. Power Sources* **2012**, *216*, 145.
[54] W. Zhang, Z. Xu, H. Li, M. Xu, S. Wang, Z. Li, A. Wang, L. Zhang, L. He, S. Li, B. Zhu, Z. Zhang, Y. Lai, *Chem. Eng. J.* **2022**, *433*, 133542.
[55] M. V. Zakharkin, O. A. Drozhzhin, I. V. Tereshchenko, A. M. Abakumov, E. V. Antipov, K. J. Stevenson, *Electrochem. Soc., Inc* **2019**, *2*, 89.
[56] S. Park, J.-N. Chotard, D. Carlier, I. Moog, M. Courty, M. Duttine, F. Fauth, A. Iadecola, L. Croguennec, C. Masquelier, *Chem. Mater.* **2021**, *33*, 5355.
[57] W. Zhang, H. Li, Z. Zhang, M. Xu, Y. Lai, S. L. Chou, *Small* **2020**, *16*, 2001524.
[58] T. Zhu, P. Hu, X. Wang, Z. Liu, W. Luo, K. A. Owusu, W. Cao, C. Shi, J. Li, L. Zhou, L. Mai, *Adv. Energy Mater.* **2019**, *9*, 1803436.
[59] F. Lalère, V. Seznec, M. Courty, J. Chotard, C. Masquelier, *J. Mater. Chem. A* **2018**, *6*, 6654.
[60] O. A. Drozhzhin, M. V. Zakharkin, V. D. Sumanov, A. V. Sobolev, I. A. Presniakov, D. Chernyshov, K. J. Stevenson, A. M. Abakumov, E. V. Antipov, *Electrochem. Soc., Inc.* **2019**, *2*, 85.
[61] D. Wang, X. Bie, Q. Fu, D. Dixon, N. Bramnik, Y.-S. Hu, F. Fauth, Y. Wei, H. Ehrenberg, G. Chen, F. Du, *Nat. Commun.* **2017**, *8*, 15888.
[62] H. Li, M. Xu, C. Gao, W. Zhang, Z. Zhang, Y. Lai, L. Jiao, *Energy Storage Mater.* **2020**, *26*, 325.
[63] P. Hu, C. Cai, X. Li, Z. Wei, M. Wang, C. Chen, T. Zhu, L. Mai, L. Zhou, *Adv. Funct. Mater.* **2023**, 2302045.
[64] R. Rajagopalan, B. Chen, Z. Zhang, X. L. Wu, Y. Du, Y. Huang, B. Li, Y. Zong, J. Wang, G. H. Nam, M. Sindoro, S.-X. Dou, H.-K. Liu, H. Zhang, *Adv. Mater.* **2017**, *29*, 1605694.
[65] Y. Cao, Y. Liu, D. Zhao, X. Xia, L. Zhang, J. Zhang, H. Yang, Y. Xia, *ACS Sustainable Chem. Eng.* **2019**, *8*, 1380.
[66] Y. Zhu, Y. Xu, Y. Liu, C. Luo, C. Wang, *Nanoscale* **2013**, *5*, 780.
[67] F. Boucher, J. Gaubicher, M. Cuisinier, D. Guyomard, P. Moreau, *J. Am. Chem. Soc.* **2014**, *136*, 9144.
[68] M. Casas-Cabanas, V. V. Roddatis, D. Saurel, P. Kubiak, J. Carretero-González, V. Palomares, P. Serras, T. Rojo, *J. Mater. Chem.* **2012**, *22*, 17421.
[69] W. Tang, X. Song, Y. Du, C. Peng, M. Lin, S. Xi, B. Tian, J. Zheng, Y. Wu, F. Pan, K.-P. Loh, *J. Mater. Chem. A* **2016**, *4*, 4882.
[70] X. Liu, J. Wang, M. Du, Q. Zhu, K. Robeyns, X. Zhang, V. Kumar, J. F. Gohy, Y. Garcia, A. Vlad, *Batteries Supercaps* **2022**, *5*, 202100390.
[71] V. Priyanka, G. Savithiri, R. Subadevi, M. Sivakumar, *Appl. Nanosci.* **2020**, *10*, 3945.
[72] R. Dima, P. Maleka, E. Maluta, R. Maphanga, *Mater Today Proc* **2022**, *62*, S7.
[73] S. P. Ong, V. L. Chevrier, G. Hautier, A. Jain, C. Moore, S. Kim, X. Ma, G. Ceder, *Energy Environ. Sci.* **2011**, *4*, 3680.
[74] P. Barpanda, S. i. Nishimura, A. Yamada, *Adv. Energy Mater.* **2012**, *2*, 841.
[75] Y. Niu, Y. Zhang, M. Xu, *J. Mater. Chem. A* **2019**, *7*, 15006.
[76] P. Barpanda, T. Ye, S.-i. Nishimura, S.-C. Chung, Y. Yamada, M. Okubo, H. Zhou, A. Yamada, *Electrochem. Commun.* **2012**, *24*, 116.
[77] H. Kim, R. Shakoor, C. Park, S. Y. Lim, J. S. Kim, Y. N. Jo, W. Cho, K. Miyasaka, R. Kahraman, Y. Jung, J. W. Choi, *Adv. Funct. Mater.* **2013**, *23*, 1147.
[78] H. Li, Z. Zhang, M. Xu, W. Bao, Y. Lai, K. Zhang, J. Li, *ACS Appl. Mater. Interfaces* **2018**, *10*, 24564.
[79] Y. Niu, M. Xu, B. Shen, C. Dai, C. M. Li, *J. Mater. Chem. A* **2016**, *4*, 16531.
[80] M. Á. Muñoz-Márquez, M. Zarrabeitia, S. Passerini, T. Rojo, *Adv. Mater. Interfaces* **2022**, 2101773.
[81] H. Li, X. Chen, T. Jin, W. Bao, Z. Zhang, L. Jiao, *Energy Storage Mater.* **2019**, *16*, 383.
[82] C. S. Park, H. Kim, R. A. Shakoor, E. Yang, S. Y. Lim, R. Kahraman, Y. Jung, J. W. Choi, *J. Am. Chem. Soc.* **2013**, *135*, 2787.
[83] P. Barpanda, M. Avdeev, C. D. Ling, J. Lu, A. Yamada, *Inorg. Chem.* **2013**, *52*, 395.
[84] J. Kim, I. Park, H. Kim, K. Y. Park, Y. U. Park, K. Kang, *Adv. Energy Mater.* **2016**, *6*, 1502147.
[85] C. Deng, S. Zhang, H. Wang, G. Zhang, *Nano Energy* **2018**, *49*, 419.
[86] C. Deng, S. Zhang, B. Zhao, *Energy Storage Mater.* **2016**, *4*, 71.
[87] H. Li, M. Xu, Z. Zhang, Y. Lai, J. Ma, *Adv. Funct. Mater.* **2020**, *30*, 2000473.
[88] R. Tripathi, S. M. Wood, M. S. Islam, L. F. Nazar, *Energy Environ. Sci.* **2013**, *6*, 2257.
[89] Q. Li, Z. Liu, F. Zheng, R. Liu, J. Lee, G. L. Xu, G. Zhong, X. Hou, R. Fu, Z. Chen, K. Amine, J. Mi, S. Wu, C. P. Gery, Y. Yang, *Angew. Chem., Int. Ed.* **2018**, *57*, 11918.
[90] S.-W. Kim, D.-H. Seo, H. Kim, K.-Y. Park, K. Kang, *Phys. Chem. Chem. Phys.* **2012**, *14*, 3299.
[91] X. Chen, Q. Wu, P. Guo, X. Liu, *Chem. Eng. J.* **2022**, 135533.
[92] Y. Yin, F. Xiong, C. Pei, Y. Xu, Q. An, S. Tan, Z. Zhuang, J. Sheng, Q. Li, L. Mai, *Nano Energy* **2017**, *41*, 452.
[93] X. Ge, X. Li, Z. Wang, H. Guo, G. Yan, X. Wu, J. Wang, *Chem. Eng. J.* **2019**, *357*, 458.
[94] M. Bianchini, N. Brisset, F. Fauth, F. Weill, E. Elkaim, E. Suard, C. Masquelier, L. Croguennec, *Chem. Mater.* **2014**, *26*, 4238.
[95] T. Broux, T. Bamine, L. Simonelli, L. Stievano, F. Fauth, M. Ménétrier, D. Carlier, C. Masquelier, L. Croguennec, *J. Phys. Chem. C* **2017**, *121*, 4103.
[96] T. Jin, Y. Liu, Y. Li, K. Cao, X. Wang, L. Jiao, *Adv. Energy Mater.* **2017**, *7*, 1700087.
[97] A. Gezović, M. J. Vujković, M. Milović, V. Grudić, R. Dominko, S. Mentus, *Energy Storage Mater.* **2021**, *37*, 243.
[98] A. Zhao, Y. Fang, X. Ai, H. Yang, Y. Cao, *J Energy Chem* **2021**, *60*, 635.

[99] H. Kim, I. Park, D.-H. Seo, S. Lee, S.-W. Kim, W. J. Kwon, Y.-U. Park, C. S. Kim, S. Jeon, K. Kang, *J. Am. Chem. Soc.* **2012**, *134*, 10369.
[100] F. Sanz, C. Parada, J. Rojo, C. Ruiz-Valero, *Chem. Mater.* **2001**, *13*, 1334.
[101] H. Kim, G. Yoon, I. Park, K.-Y. Park, B. Lee, J. Kim, Y.-U. Park, S.-K. Jung, H.-D. Lim, D. Ahn, S. Lee, K. Kang, *Energy Environ. Sci.* **2015**, *8*, 3325.
[102] M. Nose, S. Shiotani, H. Nakayama, K. Nobuhara, S. Nakanishi, H. Iba, *Electrochem. Commun.* **2013**, *34*, 266.
[103] H. Zhang, I. Hasa, D. Buchholz, B. Qin, D. Geiger, S. Jeong, U. Kaiser, S. Passerini, *NPG AsiaMater.* **2017**, *9*, e370.
[104] M. Chen, W. Hua, J. Xiao, D. Cortie, X. Guo, E. Wang, Q. Gu, Z. Hu, S. Indris, X. L. Wang, S. L. Chou, S.-X. Dou, *Angew. Chem., Int. Ed.* **2020**, *59*, 2449.
[105] H. Chen, Q. Hao, O. Zivkovic, G. Hautier, L.-S. Du, Y. Tang, Y.-Y. Hu, X. Ma, C. P. Grey, G. Ceder, *Chem. Mater.* **2013**, *25*, 2777.
[106] B. Xie, R. Sakamoto, A. Kitajou, K. Nakamoto, L. Zhao, S. Okada, Y. Fujita, N. Oka, T. Nishida, W. Kobayashi, M. Okada, T. Takahara, *Sci. Rep.* **2020**, *10*, 3278.
[107] P. Singh, S. Kumar, R. Ranjeeth, N. K. Mishra, R. Prakash, *Dalton Trans.* **2022**, *51*, 5834.
[108] Y. Kawabe, N. Yabuuchi, M. Kajiyama, N. Fukuhara, T. Inamasu, R. Okuyama, I. Nakai, S. Komaba, *Electrochem. Commun.* **2011**, *13*, 1225.
[109] Z. Jian, L. Zhao, H. Pan, Y.-S. Hu, H. Li, W. Chen, L. Chen, *Electrochem. Commun.* **2012**, *14*, 86.
[110] X. Rui, W. Sun, C. Wu, Y. Yu, Q. Yan, *Adv. Mater.* **2015**, *27*, 6670.
[111] Y. Xu, Q. Wei, C. Xu, Q. Li, Q. An, P. Zhang, J. Sheng, L. Zhou, L. Mai, *Adv. Energy Mater.* **2016**, *6*, 1600389.
[112] Y. Liu, N. Zhang, F. Wang, X. Liu, L. Jiao, L. Z. Fan, *Adv. Funct. Mater.* **2018**, *28*, 1801917.
[113] Y. Cao, X. Xia, Y. Liu, N. Wang, J. Zhang, D. Zhao, Y. Xia, *J. Power Sources* **2020**, *461*, 228130.
[114] X. Shen, Q. Zhou, M. Han, X. Qi, B. Li, Q. Zhang, J. Zhao, C. Yang, H. Liu, Y.-S. Hu, *Nat. Commun.* **2021**, *12*, 2848.
[115] G. Longoni, J. E. Wang, Y. H. Jung, D. K. Kim, C. M. Mari, R. Ruffo, *J. Power Sources* **2016**, *302*, 61.
[116] J. Yan, X. Liu, B. Li, *Electrochem. Commun.* **2015**, *56*, 46.
[117] L. Ke, T. Yu, B. Lin, B. Liu, S. Zhang, C. Deng, *Nanoscale* **2016**, *8*, 19120.
[118] W. Zhang, Z. Zhang, H. Li, D. Wang, T. Wang, X. Sun, J. Zheng, Y. Lai, *ACS Appl. Mater. Interfaces* **2019**, *11*, 35746.
[119] L. Dong, L. RuiXian, J. Feng, C. Long, G. Wang, H. Kou, M. Zhao, L. Dong, X. Li, D. Li, *Mater. Lett.* **2017**, *205*, 75.
[120] T. Sharabani, S. Taragin, I. Perelshtein, M. Noked, A. Mukherjee, *Small* **2021**, *17*, 2104416.
[121] M. Peng, B. Li, H. Yan, D. Zhang, X. Wang, D. Xia, G. Guo, *Angew. Chem., Int. Ed.* **2015**, *54*, 6452.
[122] Q. Liu, Z. Hu, W. Li, C. Zou, H. Jin, S. Wang, S. Chou, S.-X. Dou, *Energy Environ. Sci.* **2021**, *14*, 158.
[123] C. Ma, T. Xu, C. Yan, J. Xu, D. Kong, Z. Zhang, W. Shen, Y. Shi, C. Ke, X. Li, Y. Wang, *J. Power Sources* **2021**, *482*, 228906.
[124] Y. Zhu, E. Xu, J. Zhang, J. Quan, H. Wang, Z. Sun, Y. Jiang, *ACS Appl. Energy Mater.* **2021**, *4*, 3952.
[125] M. Karthik, S. Sathishkumar, R. BoopathiRaja, K. Meganathan, T. Sumathi, *J. Mater. Sci.* **2020**, *31*, 21792.
[126] R. Ling, S. Cai, D. Xie, W. Shen, X. Hu, Y. Li, S. Hua, Y. Jiang, X. Sun, *J. Mater. Sci.* **2018**, *53*, 2735.
[127] Y. Qi, L. Mu, J. Zhao, Y.-S. Hu, H. Liu, S. Dai, *J. Mater. Chem. A* **2016**, *4*, 7178.
[128] E. Wang, M. Chen, X. Liu, Y. Liu, H. Guo, Z. Wu, W. Xiang, B. Zhong, X. Guo, S. Chou, *Small Methods* **2019**, *3*, 1800169.
[129] X. Ma, X. Wu, Y. Liu, W. Wu, Z. Pan, P. K. Shen, *ACS Appl. Mater. Interfaces* **2021**, *13*, 21390.
[130] L. Wu, Y. Hu, X. Zhang, J. Liu, X. Zhu, S. Zhong, *J. Power Sources* **2018**, *374*, 40.
[131] T. Yuan, Y. Wang, J. Zhang, X. Pu, X. Ai, Z. Chen, H. Yang, Y. Cao, *Nano Energy* **2019**, *56*, 160.
[132] L. Tang, X. Liu, Z. Li, X. Pu, J. Zhang, Q. Xu, H. Liu, Y.-G. Wang, Y. Xia, *ACS Appl. Mater. Interfaces* **2019**, *11*, 27813.
[133] H. Xiong, G. Sun, Z. Liu, L. Zhang, L. Li, W. Zhang, F. Du, Z. A. Qiao, *Angew. Chem., Int. Ed.* **2021**, *60*, 10334.
[134] Q. Ni, Y. Bai, F. Wu, C. Wu, *Adv. Sci.* **2017**, *4*, 1600275.
[135] L. Xiao, F. Ji, J. Zhang, X. Chen, Y. Fang, *Small* **2023**, *19*, 2205732.
[136] H. Li, Y. Bai, F. Wu, Q. Ni, C. Wu, *ACS Appl. Mater. Interfaces* **2016**, *8*, 27779.
[137] Y. Li, M. Chen, B. Liu, Y. Zhang, X. Liang, X. Xia, *Adv. Energy Mater.* **2020**, *10*, 2000927.
[138] X. Liu, L. Tang, Z. Li, J. Zhang, Q. Xu, H. Liu, Y. Wang, Y. Xia, Y. Cao, X. Ai, *J. Mater. Chem. A* **2019**, *7*, 18940.
[139] L. Ren, L. Song, Y. Guo, Y. Wu, J. Lian, Y.-N. Zhou, W. Yuan, Q. Yan, Q. Wang, S. Ma, X. Ye, Z. Ye, J. Lu, *Appl. Surf. Sci.* **2021**, *544*, 148893.
[140] A. Inoishi, Y. Yoshioka, L. Zhao, A. Kitajou, S. Okada, *ChemElectroChem* **2017**, *4*, 2755.
[141] H. Li, H. Tang, C. Ma, Y. Bai, J. Alvarado, B. Radhakrishnan, S. P. Ong, F. Wua, Y. S. Meng, C. Wu, *Chem. Mater.* **2018**, *30*, 2498.
[142] H. Li, X. Yu, Y. Bai, F. Wu, C. Wu, L.-Y. Liu, X.-Q. Yang, *J. Mater. Chem. A* **2015**, *3*, 9578.
[143] L. Zhao, H. Zhao, Z. Du, N. Chen, X. Chang, Z. Zhang, F. Gao, A. Trenczek-Zajac, K. Świerczek, *Electrochim. Acta* **2018**, *282*, 510.
[144] Y. Zhao, X. Gao, H. Gao, H. Jin, J. B. Goodenough, *Adv. Funct. Mater.* **2020**, *30*, 1908680.
[145] M. Chen, W. Hua, J. Xiao, J. Zhang, V. W.-h. Lau, M. Park, G.-H. Lee, S. Lee, W. Wang, J. Peng, L. Fang, L. Zhou, C.-K. Chang, Y. Yamauchi, S. Chou, Y.-M. Kang, *J. Am. Chem. Soc.* **2021**, *143*, 18091.
[146] X. Liu, G. Feng, E. Wang, H. Chen, Z. Wu, W. Xiang, Y. Zhong, Y. Chen, X. Guo, B. Zhong, *ACS Appl. Mater. Interfaces* **2019**, *11*, 12421.
[147] J.-S. Park, J. Kim, J. H. Jo, S.-T. Myung, *J. Mater. Chem. A* **2018**, *6*, 16627.
[148] Y. Huang, X. Li, J. Wang, L. Miao, C. Li, J. Han, Y. Huang, *Energy Storage Mater.* **2018**, *15*, 108.
[149] C. Xu, J. Zhao, Y. A. Wang, W. Hua, Q. Fu, X. Liang, X. Rong, Q. Zhang, X. Guo, C. Yang, H. Liu, B. Zhong, Y.-S. Hu, *Adv. Energy Mater.* **2022**, *12*, 2200966.
[150] X. Ge, H. Li, J. Li, C. Guan, X. Wang, L. He, S. Li, Y. Lai, Z. Zhang, *Small* **2023**, https://doi.org/10.1002/smll.202302609.
[151] Z. Y. Gu, J. Z. Guo, J. M. Cao, X. T. Wang, X. X. Zhao, X. Y. Zheng, W. H. Li, Z. H. Sun, H. J. Liang, X. L. Wu, *Adv. Mater.* **2022**, 2110108.
[152] Y. Kawabe, N. Yabuuchi, M. Kajiyama, N. Fukuhara, T. Inamasu, R. Okuyama, I. Nakai, S. Komaba, *Electrochemistry* **2012**, *80*, 80.
[153] Y. Cao, Y. Liu, D. Zhao, J. Zhang, X. Xia, T. Chen, L.-c. Zhang, P. Qin, Y. Xia, *J. Alloys Compd.* **2019**, *784*, 939.
[154] J. Zhang, Y. Lai, P. Li, Y. Wang, F. Zhong, X. Feng, W. Chen, J. Liu, X. Ai, H. Yang, Y. Cao, *Green Energy Environ.* **2022**, *7*, 1253.
[155] Q. Zheng, X. Ni, L. Lin, H. Yi, X. Han, X. Li, X. Bao, H. Zhang, *J. Mater. Chem. A* **2018**, *6*, 4209.
[156] Y. Chen, Y. Xu, X. Sun, B. Zhang, S. He, L. Li, C. Wang, *J. Power Sources* **2018**, *378*, 423.
[157] M. J. Aragón, P. Lavela, G. F. Ortiz, R. Alcántara, J. L. Tirado, *ChemElectroChem* **2018**, *5*, 367.
[158] P. Hu, X. Wang, T. Wang, L. Chen, J. Ma, Q. Kong, S. Shi, G. Cui, *Adv. Sci.* **2016**, *3*, 1600112.
[159] Q. Wang, Q. Wang, M. Zhang, B. Han, C. Zhou, Y. Chen, G. Lv, *J Mol Model* **2019**, *25*, 1.
[160] M. Dou, Y. Zhang, J. Wang, X. Zheng, J. Chen, B. Han, K. Xia, Q. Gao, X. Liu, C. Zhou, *J. Power Sources* **2023**, *560*, 232709.
[161] Y. Liu, C. Sun, Q. Ni, Z. Sun, M. Li, S. Ma, H. Jin, Y. Zhao, *Energy Storage Mater.* **2022**, *53*, 881.

[162] G. Kucinskis, I. Nesterova, A. Sarakovskis, L. Bikse, J. Hodakovska, G. Bajars, *J. Alloys Compd.* **2022**, *895*, 162656.
[163] M. K. Sadan, H. Kim, C. Kim, S. H. Cha, K.-K. Cho, K.-W. Kim, J.-H. Ahn, H.-J. Ahn, *J. Mater. Chem. A* **2020**, *8*, 9843.
[164] D. Ba, Q. Gui, W. Liu, Z. Wang, Y. Li, J. Liu, *Nano Energy* **2022**, *94*, 106918.
[165] R. Mogensen, S. Colbin, R. Younesi, *Batteries Supercaps* **2021**, *4*, 791.
[166] H. J. Liang, Z. Y. Gu, X. X. Zhao, J. Z. Guo, J. L. Yang, W. H. Li, B. Li, Z. M. Liu, W. L. Li, X. L. Wu, *Angew. Chem., Int. Ed.* **2021**, *60*, 26837.
[167] Z. Li, Y. Zhang, J. Zhang, Y. Cao, J. Chen, H. Liu, Y. Wang, *Angew. Chem., Int. Ed.* **2022**, *61*, 2021169.
[168] Z. Li, Y. Zhang, Y. Wang, *SmartMat* **2023**, https://doi.org/10.1002/smm2.1191.
[169] S. Zhong, Y. Yu, Y. Yang, Y. Yao, L. Wang, S. He, Y. Yang, L. Liu, W. Sun, Y. Feng, *Angew. Chem., Int. Ed.* **2023**, *62*, 2023011.
[170] K. Du, C. Wang, L. U. Subasinghe, S. R. Gajella, M. Law, A. Rudola, P. Balaya, *Energy Storage Mater.* **2020**, *29*, 287.
[171] X. Liu, X. Jiang, F. Zhong, X. Feng, W. Chen, X. Ai, H. Yang, Y. Cao, *ACS Appl. Mater. Interfaces* **2019**, *11*, 27833.
[172] N. Wongittharom, T.-C. Lee, C.-H. Wang, Y.-C. Wang, J.-K. Chang, *J. Mater. Chem. A* **2014**, *2*, 5655.
[173] C. Manohar, T. C. Mendes, M. Kar, C. Xiao, M. Forsyth, S. Mitra, D. R. MacFarlane, *Chem. Commun.* **2018**, *54*, 3500.
[174] S. Lee, B. Koo, S. Kang, H. Lee, H. Lee, *Chem. Eng. J.* **2021**, *425*, 130612.
[175] J. Zhang, Y. Liu, X. Zhao, L. He, H. Liu, Y. Song, S. Sun, Q. Li, X. Xing, J. Chen, *Adv. Mater.* **2020**, *32*, 1906348.
[176] S. Altundag, S. Altin, S. Yasar, E. Altin, *Vacuum* **2023**, 111853.
[177] X. Ding, X. Huang, J. Jin, H. Ming, L. Wang, J. Ming, *Electrochim. Acta* **2018**, *260*, 882.
[178] J. Z. Guo, P. F. Wang, X. L. Wu, X. H. Zhang, Q. Yan, H. Chen, J. P. Zhang, Y. G. Guo, *Adv. Mater.* **2017**, *29*, 1701968.
[179] I. Hasa, S. Passerini, J. Hassoun, *RSC Adv.* **2015**, *5*, 48928.
[180] J. Hou, W. Wang, P. Feng, K. Wang, K. Jiang, *J. Power Sources* **2020**, *453*, 227879.
[181] P. Hu, W. Peng, B. Wang, D. Xiao, U. Ahuja, J. Réthoré, K. E. Aifantis, *ACS Energy Lett.* **2019**, *5*, 100.
[182] Y. Huang, M. Xie, Z. Wang, Y. Jiang, Y. Yao, S. Li, Z. Li, L. Li, F. Wu, R. Chen, *Small* **2018**, *14*, 1801246.
[183] J.-Y. Hwang, S.-T. Myung, J. U. Choi, C. S. Yoon, H. Yashiro, Y.-K. Sun, *J. Mater. Chem. A* **2017**, *5*, 23671.
[184] C.-H. Jo, J. U. Choi, S.-T. Myung, *J. Mater. Chem. A* **2018**, *6*, 6867.
[185] G. Yao, X. Zhang, Y. Yan, J. Zhang, K. Song, J. Shi, L. Mi, J. Zheng, X. Feng, W. Chen, *J. Energy Chem.* **2020**, *50*, 387.
[186] Q. Li, K. Jiang, X. Li, Y. Qiao, X. Zhang, P. He, S. Guo, H. Zhou, *Adv. Energy Mater.* **2018**, *8*, 1801162.
[187] S. Li, X. Song, X. Kuai, W. Zhu, K. Tian, X. Li, M. Chen, S. Chou, J. Zhao, L. Gao, *J. Mater. Chem. A* **2019**, *7*, 14656.
[188] K. Liang, S. Wang, H. Zhao, X. Huang, Y. Ren, Z. He, J. Mao, J. Zheng, *Chem. Eng. J.* **2022**, *428*, 131780.
[189] M. C. López, M. J. Aragón, G. F. Ortiz, P. Lavela, R. Alcántara, J. L. Tirado, *Chem. - Eur. J.* **2015**, *21*, 14879.
[190] X. Ma, Z. Pan, X. Wu, P. K. Shen, *Chem. Eng. J.* **2019**, *365*, 132.
[191] X. Ma, J. Xia, X. Wu, Z. Pan, P. K. Shen, *Carbon* **2019**, *146*, 78.
[192] J. Zhang, Y. Fang, L. Xiao, J. Qian, Y. Cao, X. Ai, H. Yang, *ACS Appl. Mater. Interfaces* **2017**, *9*, 7177.
[193] J. Ming, H. Ming, W. Yang, W.-J. Kwak, J.-B. Park, J. Zheng, Y.-K. Sun, *RSC Adv.* **2015**, *5*, 8793.
[194] S.-M. Oh, P. Oh, S.-O. Kim, A. Manthiram, *J. Electrochem. Soc.* **2016**, *164*, A321.
[195] W. Pan, W. Guan, S. Liu, B. B. Xu, C. Liang, H. Pan, M. Yan, Y. Jiang, *J. Mater. Chem. A* **2019**, *7*, 13197.
[196] J. Peng, J. Wang, H. Yi, W. Hu, Y. Yu, J. Yin, Y. Shen, Y. Liu, J. Luo, Y. Xu, P. Wei, Y. Li, Y. Ding, L. Miao, J. Jiang, J. Han, Y. Huang, *Adv. Energy Mater.* **2018**, *8*, 1702856.
[197] W. Ren, M. Qin, Y. Zhou, H. Zhou, J. Zhu, J. Pan, J. Zhou, X. Cao, S. Liang, *Energy Storage Mater.* **2023**, *54*, 776.
[198] W. Ren, X. Yao, C. Niu, Z. Zheng, K. Zhao, Q. An, Q. Wei, M. Yan, L. Zhang, L. Mai, *Nano Energy* **2016**, *28*, 216.
[199] Y. Tang, W. Li, P. Feng, M. Zhou, K. Wang, Y. Wang, K. Zaghib, K. Jiang, *Adv. Funct. Mater.* **2020**, *30*, 1908754.
[200] R. Thangavel, A. Samuthira Pandian, H. V. Ramasamy, Y.-S. Lee, *ACS Appl. Mater. Interfaces* **2017**, *9*, 40187.
[201] H. Wang, M. Gu, J. Jiang, C. Lai, X. Ai, *J. Power Sources* **2016**, *327*, 653.
[202] H. Wang, Y. Xiao, C. Sun, C. Lai, X. Ai, *RSC Adv.* **2015**, *5*, 106519.
[203] H. Wang, E. Xu, S. Yu, D. Li, J. Quan, L. Xu, L. Wang, Y. Jiang, *ACS Appl. Mater. Interfaces* **2018**, *10*, 34222.
[204] L. Wang, Y. Ni, K. Lei, H. Dong, S. Tian, F. Li, *ChemSusChem* **2018**, *11*, 3376.
[205] W. Wang, L. Shi, D. Lan, Q. Li, *J. Power Sources* **2018**, *377*, 1.
[206] Z. Wang, Y. Huang, R. Luo, F. Wu, L. Li, M. Xie, J. Huang, R. Chen, *J. Power Sources* **2019**, *436*, 226868.
[207] Y. Xu, J. Wan, L. Huang, M. Ou, C. Fan, P. Wei, J. Peng, Y. Liu, Y. Qiu, X. Sun, Q. Li, J. Han, Y. Huang, J. A. Alonso, Y. Zhao, *Adv. Energy Mater.* **2019**, *9*, 1803158.
[208] D. Yang, J. Xu, X.-Z. Liao, Y.-S. He, H. Liu, Z.-F. Ma, *Chem. Commun.* **2014**, *50*, 13377.
[209] Q. Yang, P.-F. Wang, J.-Z. Guo, Z.-M. Chen, W.-L. Pang, K.-C. Huang, Y.-G. Guo, X.-L. Wu, J.-P. Zhang, *ACS Appl. Mater. Interfaces* **2018**, *10*, 34272.
[210] X. Yang, R. Y. Zhang, J. Zhao, Z. X. Wei, D. X. Wang, X. F. Bie, Y. Gao, J. Wang, F. Du, G. Chen, *Adv. Energy Mater.* **2018**, *8*, 1701827.
[211] K. Zhu, S. Guo, J. Yi, S. Bai, Y. Wei, G. Chen, H. Zhou, *J. Mater. Chem. A* **2015**, *3*, 22012.
[212] C.-D. Zhao, J.-Z. Guo, Z.-Y. Gu, X.-X. Zhao, W.-H. Li, X. Yang, H.-J. Liang, X.-L. Wu, *J. Mater. Chem. A* **2020**, *8*, 17454.
[213] Z. Yang, J. He, W. H. Lai, J. Peng, X. H. Liu, X. X. He, X. F. Guo, L. Li, Y. Qiao, J. M. Ma, M. Wu, S. L. Chou, *Angew. Chem., Int. Ed.* **2021**, *60*, 27086.
[214] A. Zhao, C. Liu, F. Ji, S. Zhang, H. Fan, W. Ni, Y. Fang, X. Ai, H. Yang, Y. Cao, *ACS Energy Lett.* **2022**, *8*, 753.
[215] H. Zhang, Y. Gao, X. Liu, L. Zhou, J. Li, Y. Xiao, J. Peng, J. Wang, S. L. Chou, *Adv. Energy Mater.* **2023**, https://doi.org/10.1002/aenm.202300149.

Zhiqiang Hao received his Ph.D. degree (2021) from the Department of Chemical Engineering, Faculty of Engineering, Kyushu University. After that, he works as a postdoctoral researcher at the Institute for Carbon Neutralization, College of Chemistry and Materials Engineering, Wenzhou University. His research mainly focuses on preparing electrode active materials for sodium-ion batteries.

Lin Li is an Oujiang Distinguished Professor and associate dean of the Institute for Carbon Neutralization, College of Chemistry and Materials Engineering, Wenzhou University. He received his B.S. degree in materials science and engineering from Nanchang University (2016). He obtained his Ph.D. from Nankai University in 2021. His research focuses on advanced electrode materials and electrolyte for lithium-ion batteries, sodium-ion batteries and potassium-ion batteries.